SLAC-PUB-2813
September 1981
(T/E)

EARLY RESULTS FROM THE MKII DETECTOR AT PEP*

Jonathan Dorfan
Stanford Linear Accelerator Center
Stanford University, Stanford, California 94305

ABSTRACT

Preliminary PEP results from the MKII detector are presented based on an integrated luminosity of 15.4 pb^{-1}. All data are at the center-of-mass energy ($E_{c.m.}$) of 29 GeV. General characteristics of the one-photon annihilation data include (among other things) measurements of R, $\langle n \rangle_{charged}$, inclusive momentum distributions for hadrons and K^0's and evidence for broad (high sphericity) planar events. These results are qualitatively in good agreement with those of the PETRA experiments. Comparisons between inclusive momentum distributions from MKII data taken at SPEAR ($E_{c.m.}$ = 5.2 GeV) and PEP ($E_{c.m.}$ = 29 GeV) imply sizeable scaling violations in x (= $2P/E_{c.m.}$). Diparticle energy correlations have been studied yielding fully corrected model independent measurements for comparison with QCD models. A comparison with one such first order calculation yields a result for the strong coupling constant, α_s. A cluster algorithm has been used to study multijet topologies and in particular the three-jet topology yields a measurement of the gluon spin and a test of gluon fragmentation. The first positive measurement of the τ lifetime is presented which agrees with the expectation from e-μ-τ universality of the weak charged current. From e-μ events upper limits are placed on the mass of a new heavy lepton as well as a spin-0 boson. Using the reaction $e^+e^- \to \gamma\gamma$ stringent tests of QED scale breaking

---

* Work supported by the Department of Energy, contract DE-AC03-76SF00515.

Presented at the SLAC Summer Institute on Particle Physics, Stanford, California, July 17-August 7, 1981.

are presented. Effects of Z^0 exchange are studied using the reactions $e^+e^- \to e^+e^-$ and $e^+e^- \to \mu^+\mu^-$ which yield measurements of the weak coupling constants g_A^2 and g_V^2.

INTRODUCTION

The physics of e^+e^- at the storage rings PEP and PETRA was expected to be dominated by the discovery and subsequent study of the t quark. Experiments at PETRA[1] have been able to rule out the presence of the t quark up to masses on the order of 19 GeV. Since then the focus of 30 GeV e^+e^- physics has shifted towards the study of QCD (jets), QED at high q^2, electroweak phenomena and, more recently, two-photon physics. The early MKII data presented below[2] will cover all but the last of these topics. In addition a significant new contribution is presented--the first positive measurement of the τ lifetime has been made.

The PEP storage ring has been delivering reliable physics beams since about February 1981. The majority of the data presented herein was collected during the months of April through June 1981. Hence, there has been very little time to process and analyze these data and the results should be treated as preliminary with confirmation publications to follow soon. Despite the short elapsed time since the data taking, significant physics results have emerged which were made possible by the fact that the MKII detector at PEP is essentially unchanged from its configuration at SPEAR. A complete description of the MKII at SPEAR can be found in Ref. 3. The only PEP additions to the MKII pertinent to the results herein are the addition of four drift chamber layers (the so-called trigger chamber) between the beam pipe and the central drift chamber and the inclusion of extra layers of steel to the muon system.

The addition of the trigger chamber is important for the study of the τ lifetime as it improves our decay length resolution by 30-50%. The momentum resolution of the trigger chamber/drift chamber combination is $\sigma_P \simeq 0.6\% \ P^2$ (P in GeV/c) for tracks constrained to the beam crossing point and 0.8% P for unconstrained tracks. These resolutions have been obtained from $e^+e^- \to \mu^+\mu^-$ events at $E_{c.m.} = 29$ GeV. The MKII trigger at PEP is an "OR" of three basic triggers: the charged particle trigger, the neutral trigger and a small angle Bhabha trigger. Every sixteenth small angle Bhabha trigger is accepted and logged out to tape. In this way we are able to study the small angle luminosity monitor for possible systematic problems. The charged trigger requires at least two charged tracks with $P_\perp \gtrsim 100$ MeV/c and $\cos\theta \lesssim 0.8$. For the neutral trigger we form an analog sum of the liquid argon strip signals for each module. We place a 1 GeV threshold (per module) on this summed signal and require at least two modules in coincidence. This trigger has been used for the study of $e^+e^- \to \gamma\gamma$. Because wide angle Bhabhas generate both a charged and neutral trigger we are able to check the neutral trigger efficiency for $e^+e^- \to \gamma\gamma$ in a very natural way. For typical PEP luminosities of 6×10^{30} cm^2 sec^{-1}, the MKII trigger rate is $\sim$ 1.5 Hz--about 70% of which comes from the charged trigger.

The results presented below are based on all MKII data which have been logged to date. They comprise an integrated luminosity of 15.4 pb^{-1}, all at $E_{c.m.} = 29$ GeV. Simulation of the detector, necessary for the understanding and correction of the data, is done by creating raw data and passing these raw data through the identical software chain as the real data. In this way any problems associated with the software are accounted for in the Monte Carlo data. Various Monte Carlo models are

available in the MKII simulation package--however for the data presented below the model of Ali et al.[4] has been used exclusively. We have not had time to obtain an optimal set of simulation parameters for this model--however the reconstructed Monte Carlo event distributions agree well with the data. For reference we have used the following values for the standard parameters: $\alpha_s = 0.185$, $\sigma_q = 300$ MeV/c, $P/P+V = 0.66$ and $a_f = 0.7$. Here P/V is the ratio of pseudoscalar to vector mesons, a_f is the constant in the longitudinal quark fragmentation function (Feynman-Field is used), σ_q pertains to the transverse fragmentation and α_s is the strong coupling constant. Fig. 1, shows a comparison between the Monte Carlo simulation and the data for the observed charged multiplicity [1(a)] and the fractional energy seen on the MKII [1(b)]. The intent of these comparisons is to establish that the simulation is good and that we are therefore justified in using the Monte Carlo program to obtain corrected data. We have assigned a systematic error of 7% to the corrections involved in measurements such as R. This (large) systematic error will go down as soon as we have time to optimize the model parameters. The luminosity is measured in the MKII in a standard way. Small angle Bhabha scattering is measured and a cross-check is performed using the wide angle Bhabhas as measured by the liquid argon calorimeters. Again time has limited the extent to which we have performed this check and as of now we believe that our luminosity measurement is good to 5%. (It is hoped that this will soon be reduced to 2%.)

STUDIES OF HADRONIC ONE PHOTON ANNIHILATION EVENTS

Although each analysis of the one photon annihilation events differs slightly, they all use the basic set of cuts which is described below.

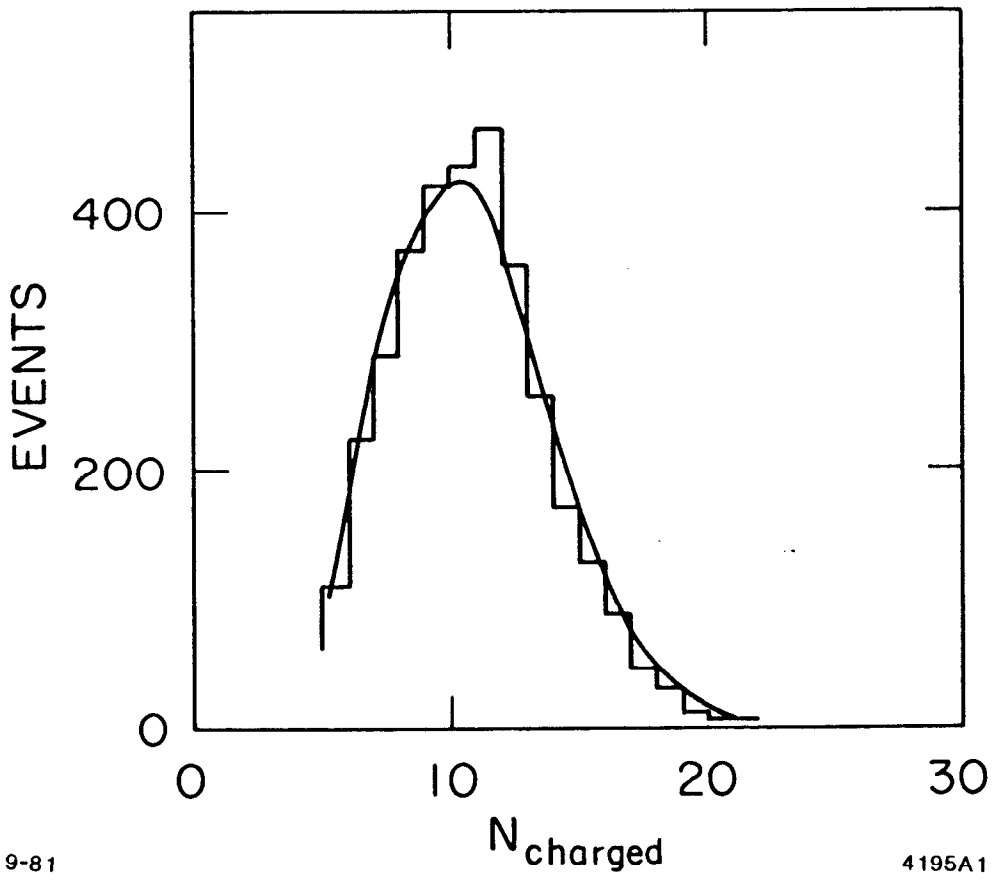

Fig. 1(a). The charged particle multiplicity for the hadronic events selected as described in the text is shown in the histogram. The solid line is the prediction of the Monte Carlo simulation program.

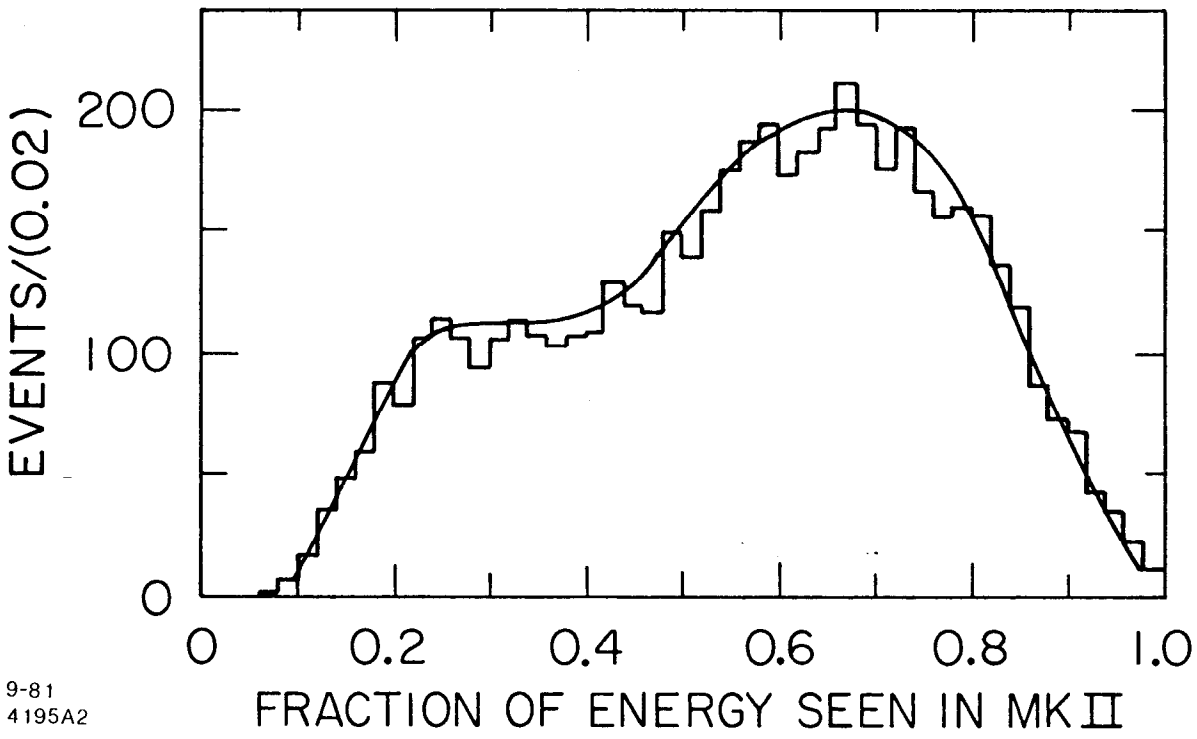

Fig. 1(b). The histogram shows the fraction of energy, charged plus neutral, observed in the MKII for the hadronic event sample. The solid line is the prediction of the Monte Carlo simulation program.

Unless important, deviations from these basic cuts will not be described. This method of presenting the data will be less confusing and the reader will not be short-changed by the omission of small changes from the cuts which follow. There are three obvious sources of background to the hadronic one photon annihilation channel in e^+e^-: beam gas events, τ hadronic decays, and events arising from two photon exchange. The best way to reject these backgrounds (without much loss to the signal) is to require a fairly large charged multiplicity in conjunction with the observation in the detector of a large fraction of the center-of-mass energy. Charged particles are required to have momenta > 100 MeV/c and to emanate from the luminous spot. Photons are detected in the liquid argon barrel modules and are required to have energies above 200 MeV. For charged and neutral particles thus defined, a simple set of cuts is made. We require at least five charged particles which must define an acceptable vertex. The vertex cuts are $|Z|$ (along the beam direction) < 7 cm and r < 4 cm. In addition we require that the energy in charged particles plus neutrals be at least 50% of $E_{c.m.}$. With these cuts the backgrounds are held to be less than 2%. The background from beam gas events has been measured using the charged vertex Z and r distributions and those from τ decays and two-photon physics estimated from Monte Carlo simulations.

We have measured R, the ratio of the hadronic production section and the mu pair cross section. In principle this is an easy measurement to make--one merely counts hadronic events and normalizes to the corresponding integrated luminosity. In practice one has to correct for initial state radiation, uninstrumented portions of the solid angle, uncertainties in the luminosity and losses due to event selection cuts. The MKII

trigger is very loose (two charged particles) and, given that the mean charged multiplicity is twelve, creates no bias. The selection cuts discussed above isolate 3430 hadronic events. Using the Monte Carlo simulation program we obtain a radiatively corrected efficiency $\epsilon = 0.53$. Combining these numbers with the integrated luminosity yields

$$R = 4.02 \pm 0.10 \pm 0.35 \quad .$$

The systematic error is a quadratic addition of 5% for the luminosity and 7% for the efficiency. The large uncertainty in the efficiency arises from the fact that we have not had time to understand fully the model dependence of this correction. The value of R is in excellent agreement with the results from PETRA.[4] For the five quarks u,d,s,c and b the naive quark-parton model prediction for R is 3.67. QCD corrections[5] move this up to 4. Addition of a t quark would add a $\Delta R = 1.33$ and hence R would be ~ 5.3. The data clearly favor the absence of the t quark at 29 GeV. As we will see below the mean sphericity is a much more sensitive measure of whether one has reached t quark threshold. We have measured the mean charge multiplicity and again find a result in good agreement with the PETRA results:[4]

$$\langle n \rangle_{\text{charged}} = 12.0 \pm 0.6 \pm 1.2 \quad .$$

This measurement is corrected for all detector biases.

We have used the standard sphericity (momentum tensor) analysis[6] to study the shape of the hadronic events. We find a mean sphericity of

$$\langle s \rangle = 0.130 \pm 0.003 \quad .$$

Again this result is corrected for all detector biases and can be compared with the corrected result of TASSO,[7] namely $\langle s \rangle = 1.346 \pm 0.076$ at

$E_{c.m.}$ = 29 GeV. If 29 GeV were above the treshold for $t\bar{t}$, one would expect an average sphericity of ~ 0.24. Hence the above measurement is a clear indication from the MKII at PEP that the $t\bar{t}$ threshold is above 29 GeV.

We have investigated the momentum transverse to the sphericity axis and find qualitative agreement with the PETRA results. Fig. 2 shows the $\langle P_\perp^2 \rangle$ distribution, where the average is formed using all particles in an event. This distribution is shown for particles projected into the event plane ($\langle P_\perp^2 \rangle_{IN}$) and transverse to the event plane ($\langle P_\perp^2 \rangle_{out}$). One clearly sees the now characteristic feature of the PETRA/PEP hadronic events--namely they are planar structures with limited momentum out of the event plane. In addition the long tail of the $\langle P_\perp^2 \rangle_{IN}$ distribution cannot be fit by a model in which one has pure $q\bar{q}$ production and Feynman-Field type fragmentation. This is true even if one allows σ_q to grow arbitrarily large. One can obtain the same conclusion from looking at the sphericity distribution. The addition of gluon bremsstrahlung, as in our Monte Carlo of Ali et al.[8] accounts qualitatively rather well for the observed event shapes. Explicit three-jet events are discussed later.

We have made a careful comparison between inclusive momentum distributions as measured by the MKII at SPEAR and PEP and are led to the conclusion that there are sizeable scale violations in $x(2P/E_{c.m.})$. Fig. 3(a) shows $sd\sigma/dx$ for charged particles as measured by the MKII at 29 GeV (PEP). These data are corrected for detector inefficiencies. Also shown on Fig. 3(a) are the corrected data of TASSO[7] which agree extremely well (within statistics in fact) with the MKII data. [Statistical errors only are shown on Figs. 3(a)-3(c)]. For the MKII the

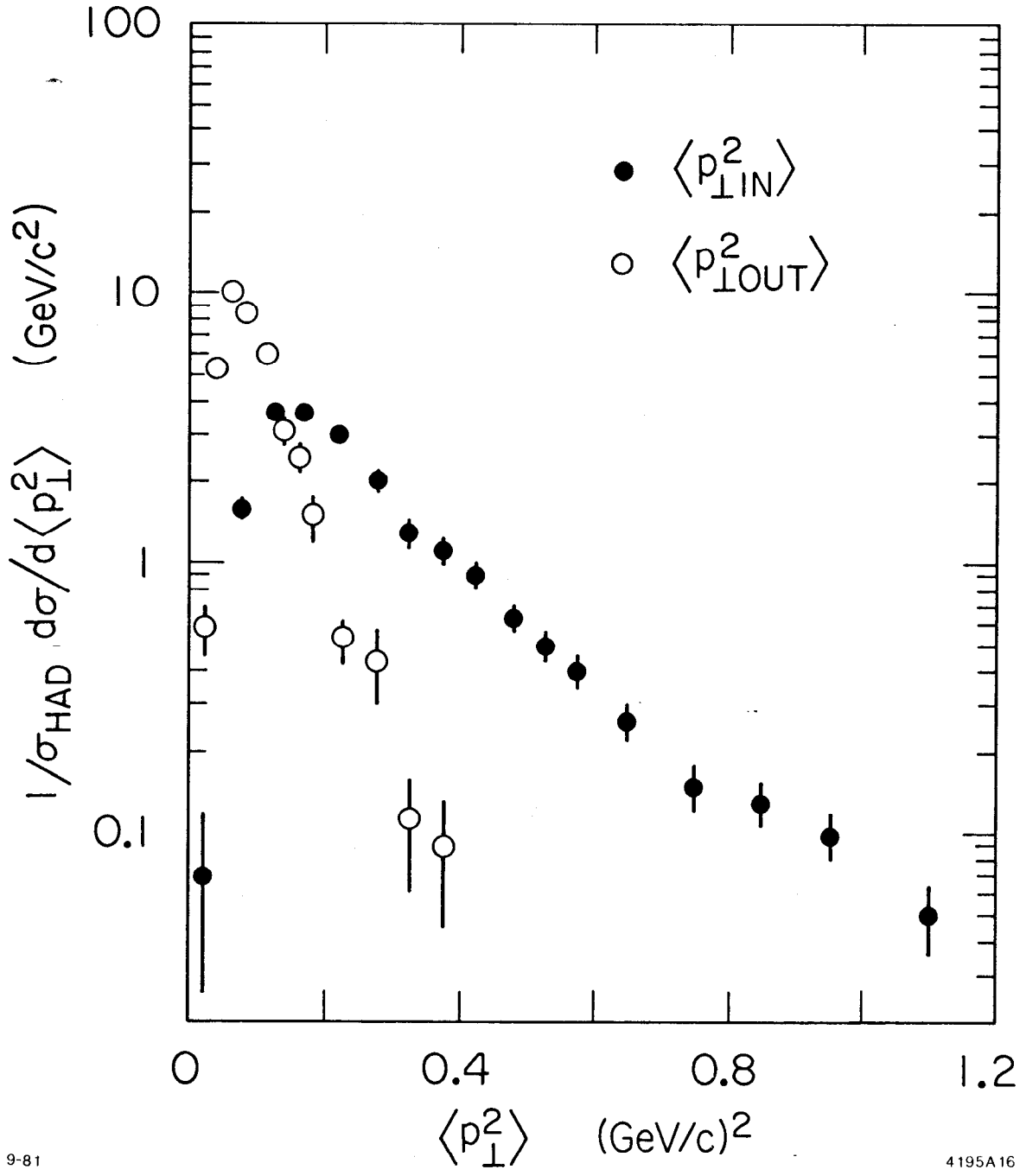

Fig. 2. The average transverse momentum squared relative to the sphericity axis, calculated per event is shown. The solid dots represent $\langle P_\perp^2 \rangle$ in the event plane; the open dots are $\langle P_\perp^2 \rangle$ normal to the event plane.

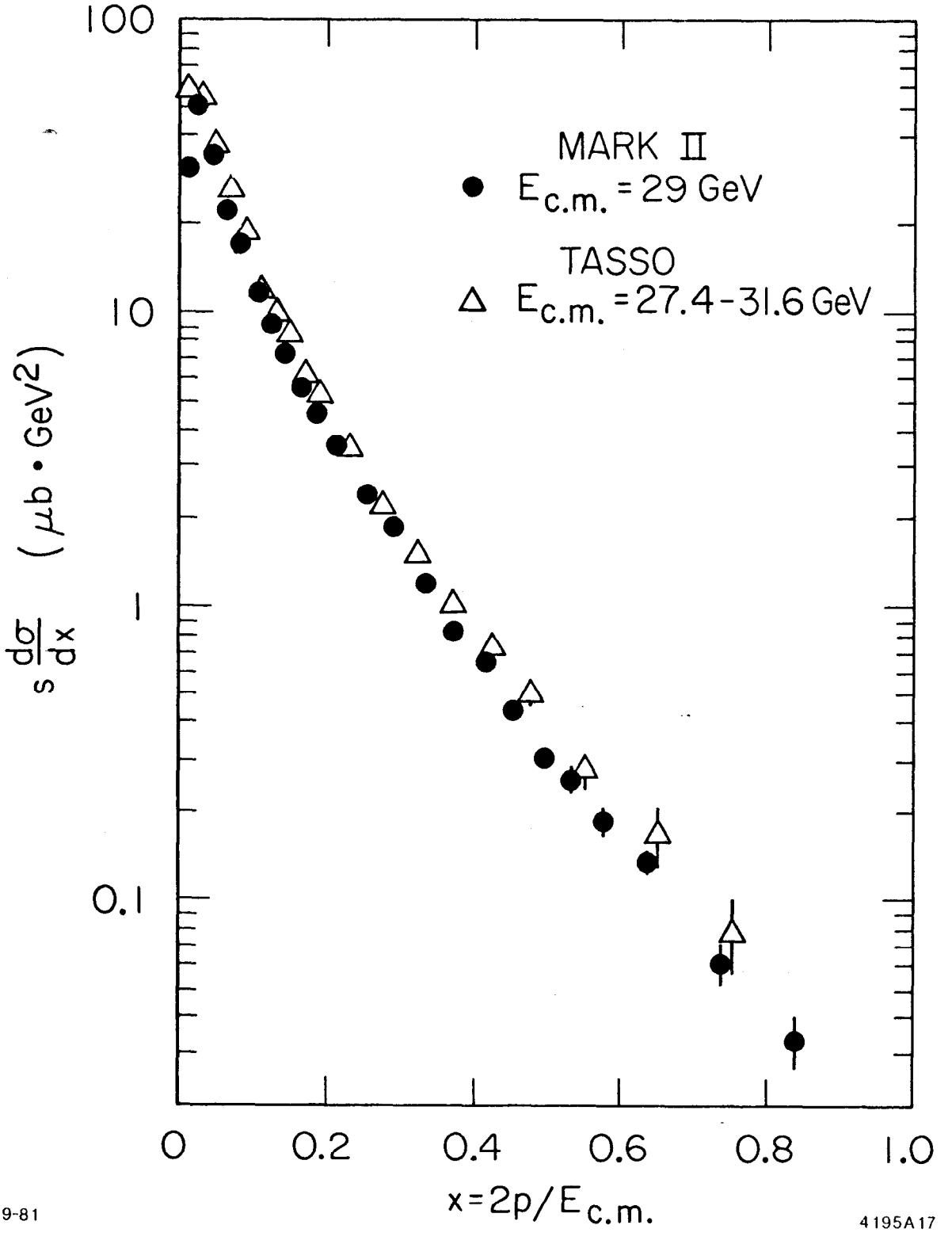

Fig. 3(a). The invariant cross section s dσ/dx ($x = 2P/E_{c.m.}$) is shown for different experiments. The MKII at $E_{c.m.}$ = 29 GeV is compared with TASSO ($27.4 < E_{c.m.} < 31.5$ GeV).

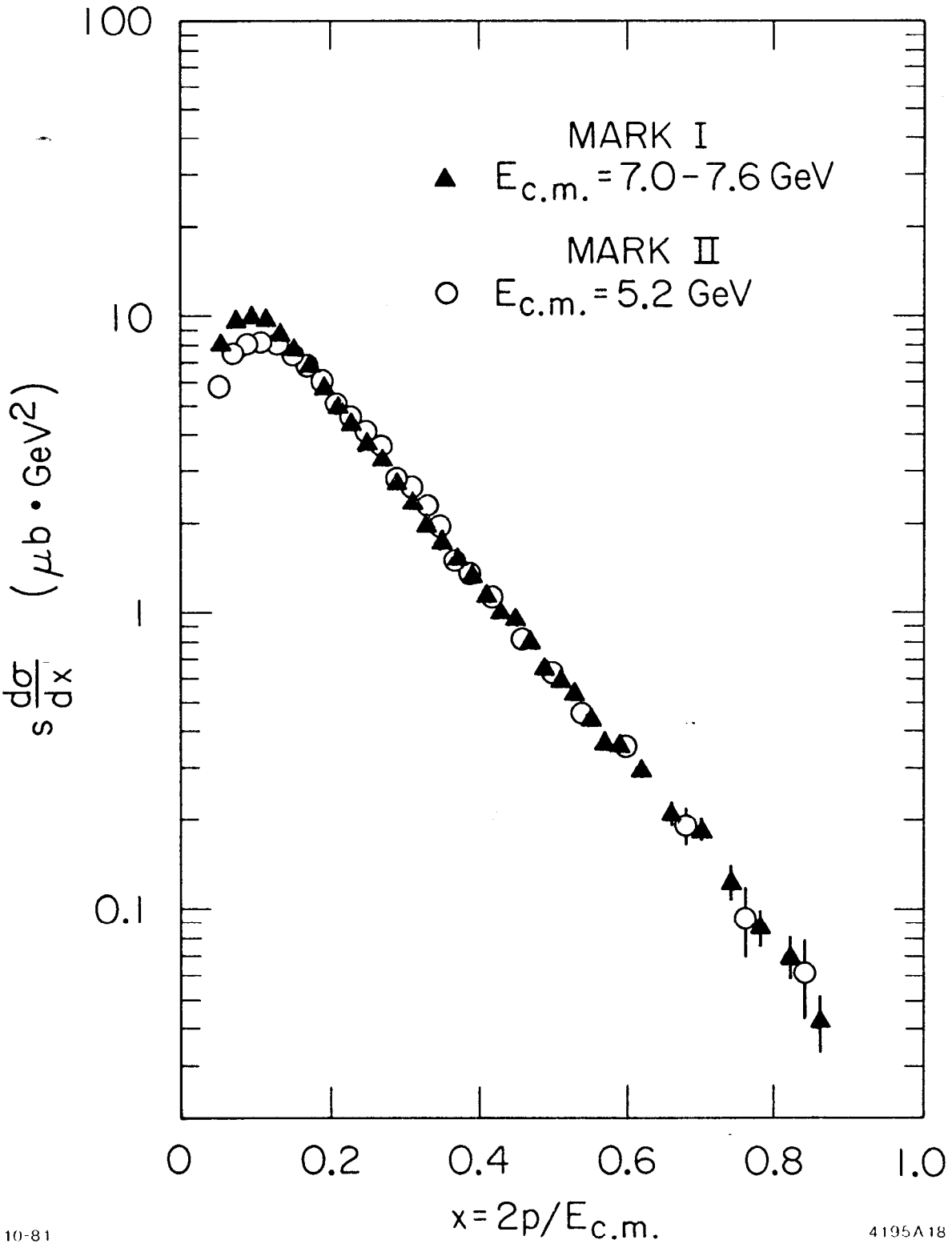

Fig. 3(b). The invariant cross section s $d\sigma/dx$ ($x = 2P/E_{c.m.}$) is shown for different experiments. The MKII at $E_{c.m.} = 5.2$ GeV is compared with the MKI ($7.0 < E_{c.m.} < 7.6$ GeV).

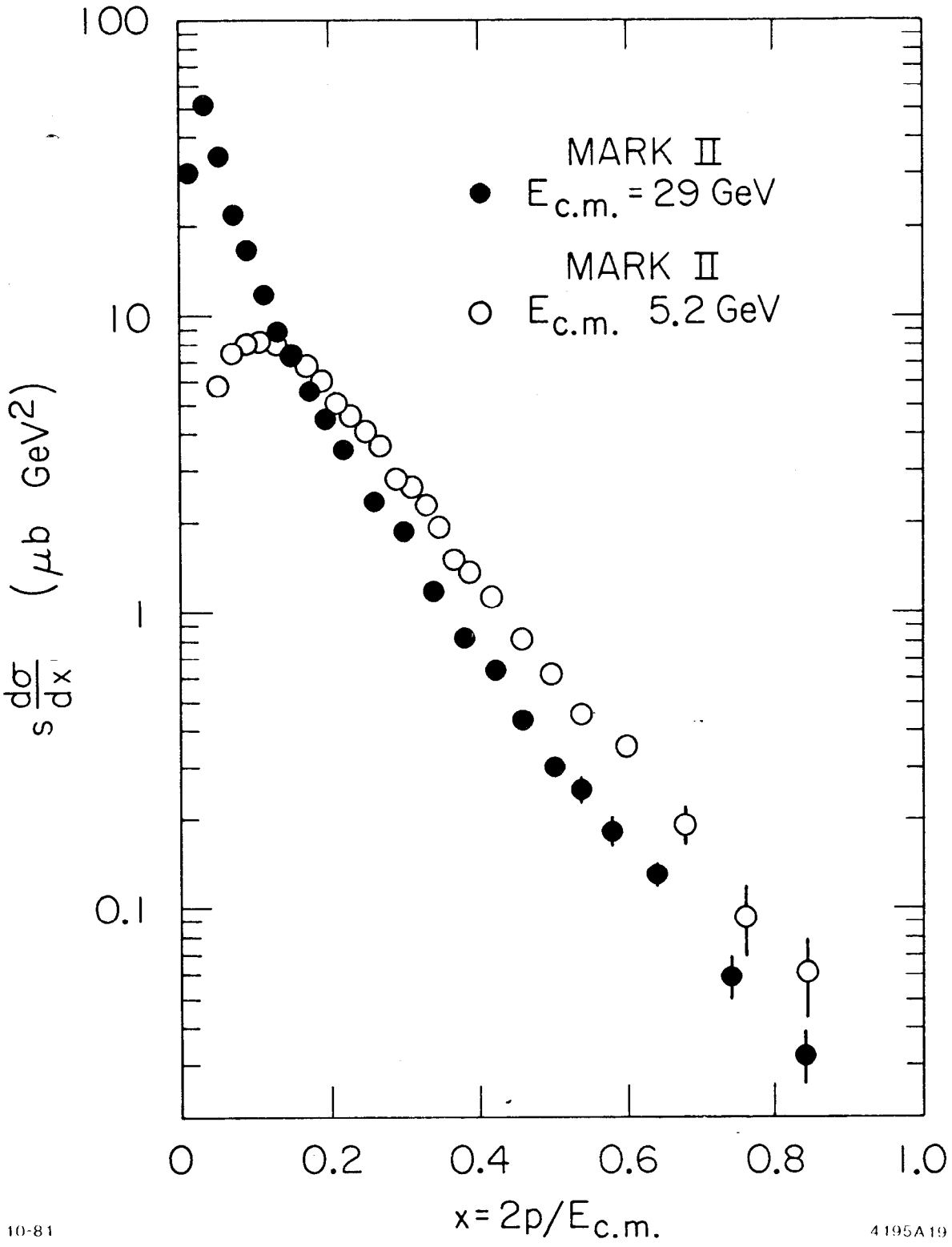

Fig. 3(c) The invariant cross section s $d\sigma/dx$ ($x = 2P/E_{c.m.}$) is shown for differnt experiments. The MKII at $E_{c.m.}$ = 29 GeV is compared with the MKII at 5.2 GeV. We see sizeable scaling violations for $x \gtrsim 0.3$.

systematic errors are on the order of 15%. Fig. 3(b) contrasts the MKII at $E_{c.m.} = 5.2$ GeV (SPEAR) with the MKI at $E_{c.m.} = 7.0$-7.6 GeV. Both sets of data have been corrected for detector inefficiencies. The agreement between the MKI and MKII is excellent. Finally Fig. 3(c) compares the MKII at 5.2 GeV and 29 GeV. One confirms the PETRA result that most of the increase in multiplicity in going from 5 GeV-30 GeV is in soft particles. In addition we observe large scale violations for $X \gtrsim 0.3$--there is almost a factor of two difference in the particle yield at the two energies for $X \sim 0.4$. This is far beyond the systematics which are on the order of 15% at each energy. The agreement between the MKII and TASSO at high energy and between the MKI and MKII at low energy lead us to the conclusion that the scale violations seen in Fig. 3(c) are not an artifact of the data analyses, but a real physics effect. Scale violations are expected in QCD because of the emission of gluons by the quarks which soften the inclusive momentum distribution. However, it is still to be seen whether the large scaling violations which are observed can be fit by QCD.

In the above discussion of $sd\sigma/dx$ all charged particles are used with no attempt at separating the hadrons into particle types. Reconstructed $K^0_s \to \pi^+\pi^-$ decays have been used to study the inclusive distribution of strange hadrons. K^0_s's are found by standard verticizing techniques--the vertex being defined by the point of closest approach between a pair of oppositely charged particles. The momentum vector of the particle pair is required to point back to the interaction point within 0.5 cm. To reduce backgrounds, both tracks are required to have their point of closest approach > 0.25 cm from the e^+e^- interaction point. K^0_s's are defined as particle pairs satisfying the above critera as well as

having their mass in the range 0.475-0.525 GeV/c^2 and their proper time greater than 0.5 cm. Fig. 4 shows the invariant mass distribution from which the K^o_s signal is derived. The radiatively corrected efficiency as a function of momentum is shown in Fig. 5. This efficiency is obtained by running Monte Carlo events through the same analysis program as the data. We observe 583 $K_s \to \pi^+\pi^-$ decays of which 166 are estimated to be background. Doing a (momentum) bin-by-bin correction for the detection efficiency, correcting for the unseen K^o_s decays and assuming equal K^o_L and K^o_s we obtain a neutral kaon cross section of $\sigma = (0.54 \pm 0.04)$ nb and find 1.3 ± 0.1 neutral kaons/event. The errors quoted are statistical--systematic errors arising from the luminosity and the efficiency corrections are estimated to be 10%. Fig. 6 shows $sd\sigma/dx$ for the neutral kaons as well as for all charged hadrons. The yield of neutral kaons (and hence presumably the charged kaons) relative to all charged hadrons is ~ 16%--with no indication of a strong x dependence to this yield.

MULTIJET TOPOLOGIES USING A CLUSTER ALGORITHM

The presence of three (and four) jet events at PEP/PETRA energies is presumed to be due to the onset of gluon bremsstrahlung in accordance with the expectations of QCD. QCD models, as manifested in Monte Carlo simulations,[8] have done an excellent job of accounting for most quantitative features of PETRA data.[9] These models include all first order effects and, in some cases, second order effects. Three jet events, in particular, are considered prime evidence for the existence of gluons. However, it is important that a test as fundamental as this go beyond comparisons between data and Monte Carlo simulations, and people have sought more direct manifestations of gluons. Those studies have

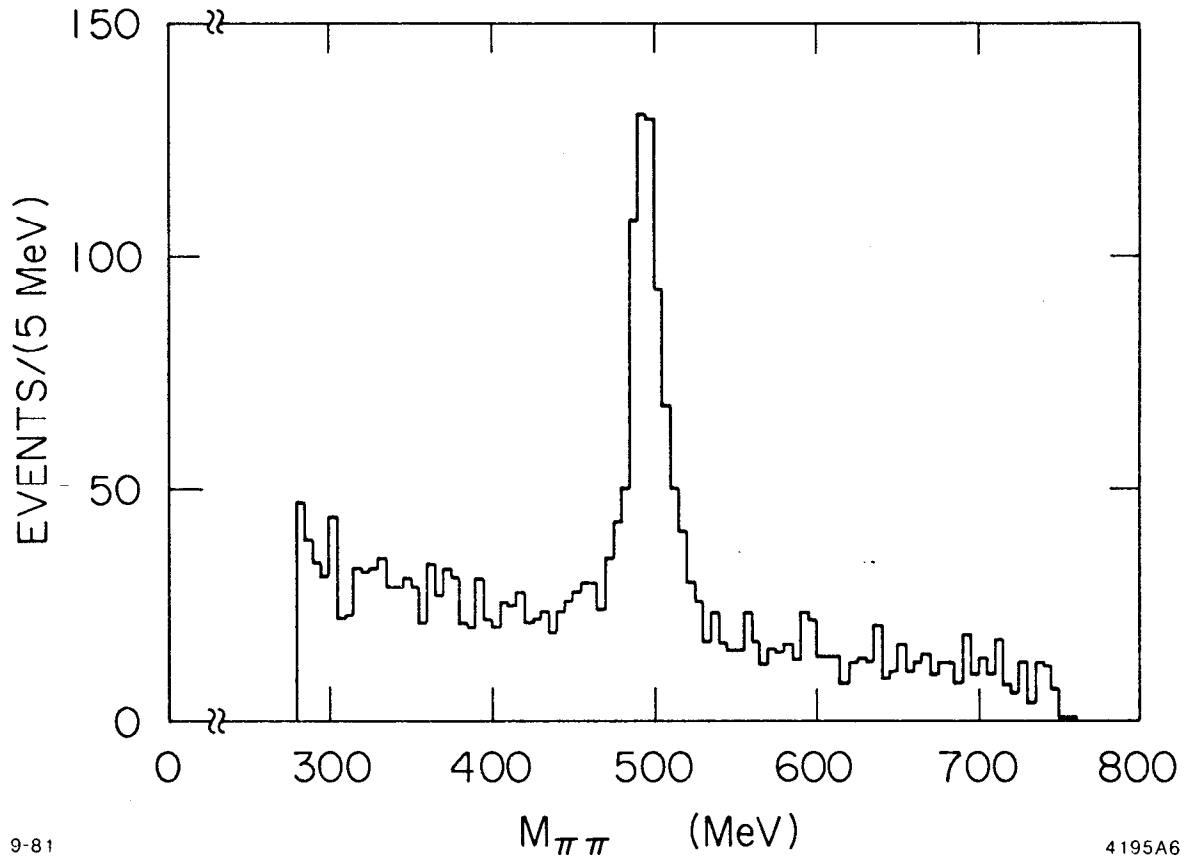

Fig. 4. The $\pi\pi$ invariant mass for hadronic events is shown. A clear signal at the K^0_S mass is seen.

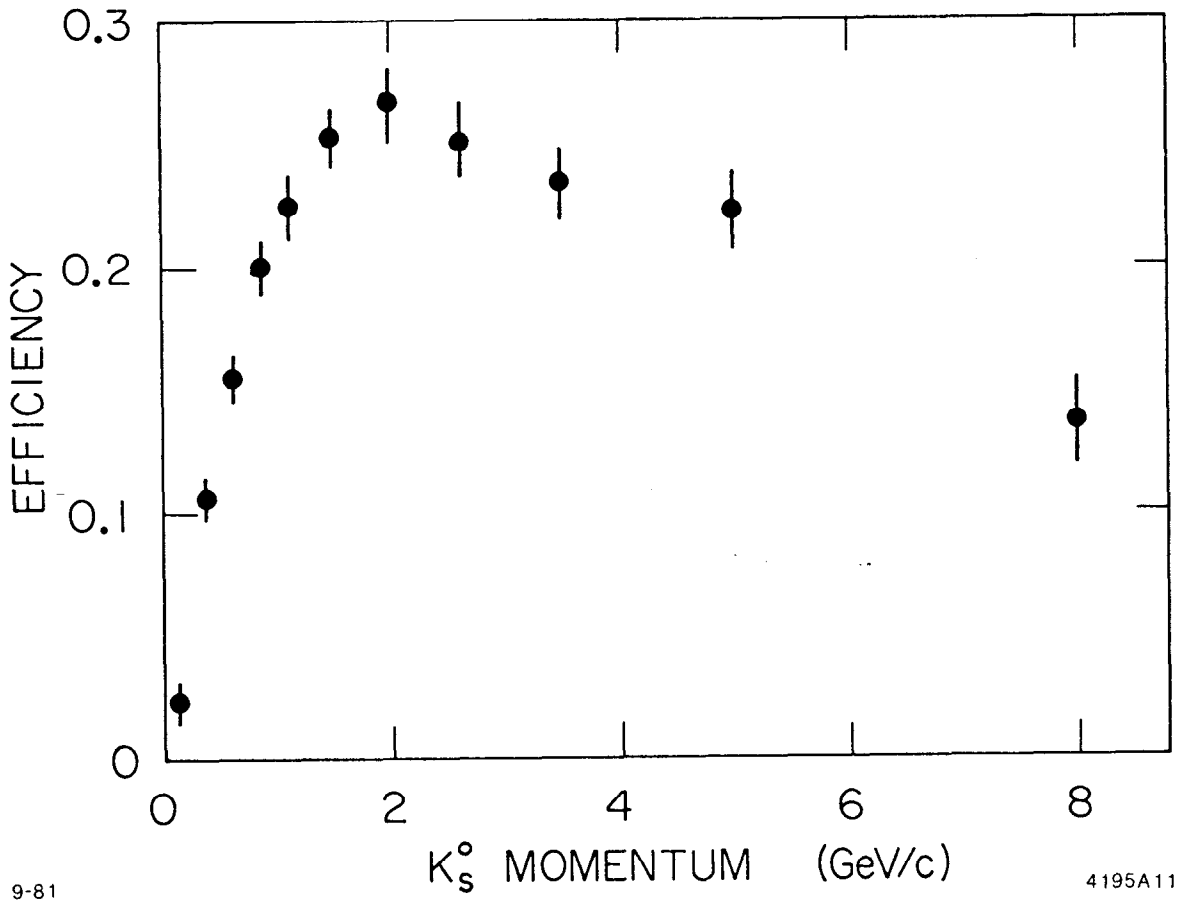

Fig. 5. The K_S^0 detection efficiency is shown as a function of the K_S^0 momentum.

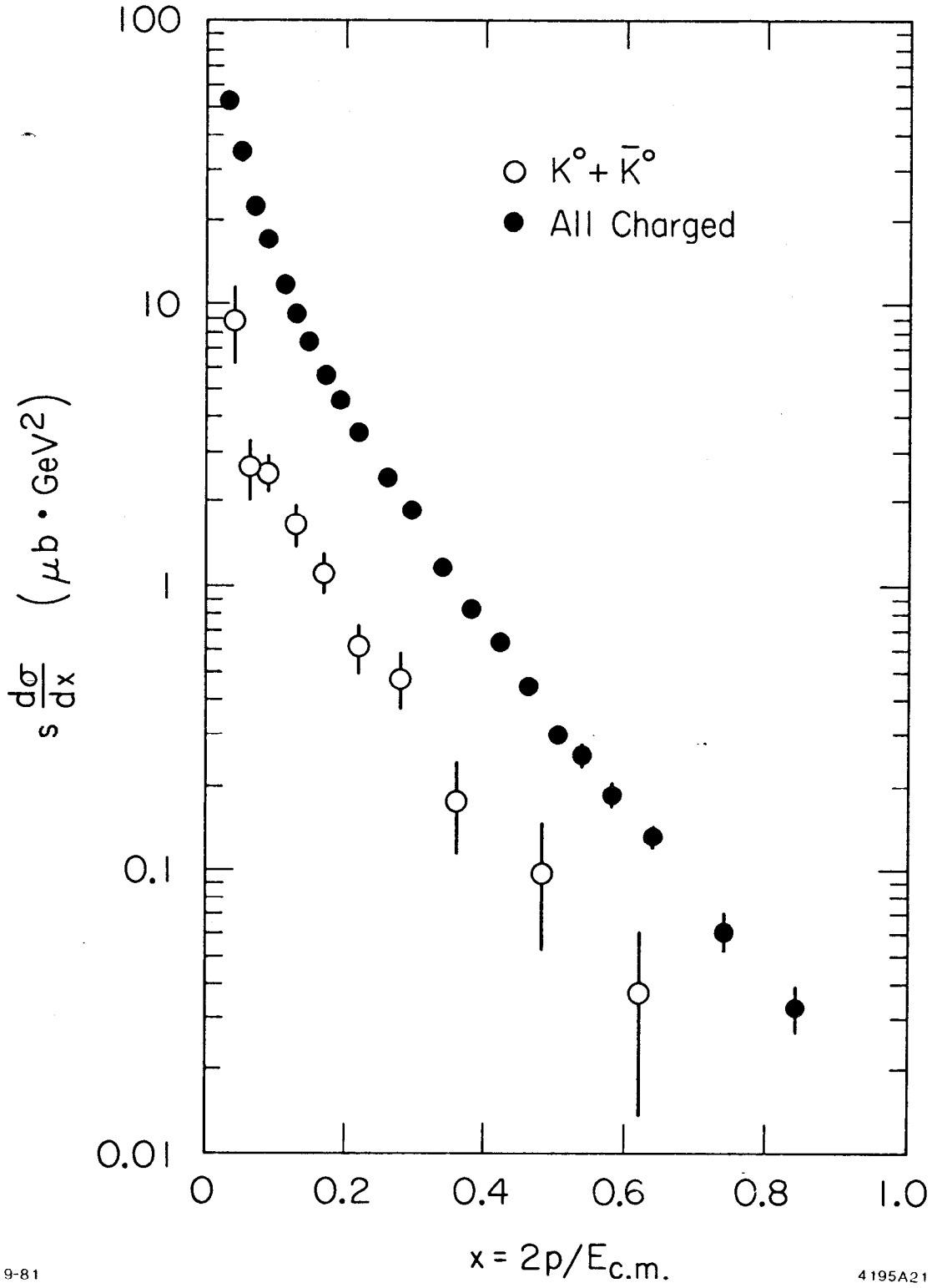

Fig. 6. This figure compares the invariant cross section s dσ/dx for K°'s (open dots) and all hadrons (solid dots). The K°'s are ~ 16% of the hadrons with little x variation.

concentrated on the well identified three-jet events. Algorithms for the study of the three-jet events have evolved of which triplicity,[10] trijettiness[11] and oblateness[12] are the three most widely used methods. These methods have the disadvantage of being constructed specifically to find planar, three-jet events and in this sense they are biased in favor of the desired result. They require the use of a shape analysis (sphericity, thrust) in order to make event selections prior to the application of the three-jet algorithm and hence they do not have a natural association with the two (or four) jet events which are found by different algorithms. If multijet topologies do indeed exist, these should result in particle direction correlations and hence clusters. There are several cluster algorithms in the literature[13,14,15] of which two[14,15] have been applied to PEP/PETRA physics analysis. The analysis described below uses the cluster algorithm described in reference 14. The cluster algorithms are applied to all selected hadronic events and sort events by their cluster (jet) number. In this way a single algorithm handles the 2,3,4 ... n jet topologies. In the case of the mimimal spanning tree (MST) algorithm used below, two cuts suffice to sort the events into clusters. A detailed description of the MST algorithm can be found in Ref. 14; a brief description follows below.

A cluster in a hadronic e^+e^- event is loosely defined as a set of particles which are correlated in direction and anticorrelated in direction with the other particles in the event. The MST algorithm finds clusters as follows. Imagine for the moment a set of space points a,b,c ... p as shown in Fig. 7(a). If we define a measure of distance (i.e., a metric) for this space, we can imagine constructing a set of interconnections between these space points (a tree) such that the tree

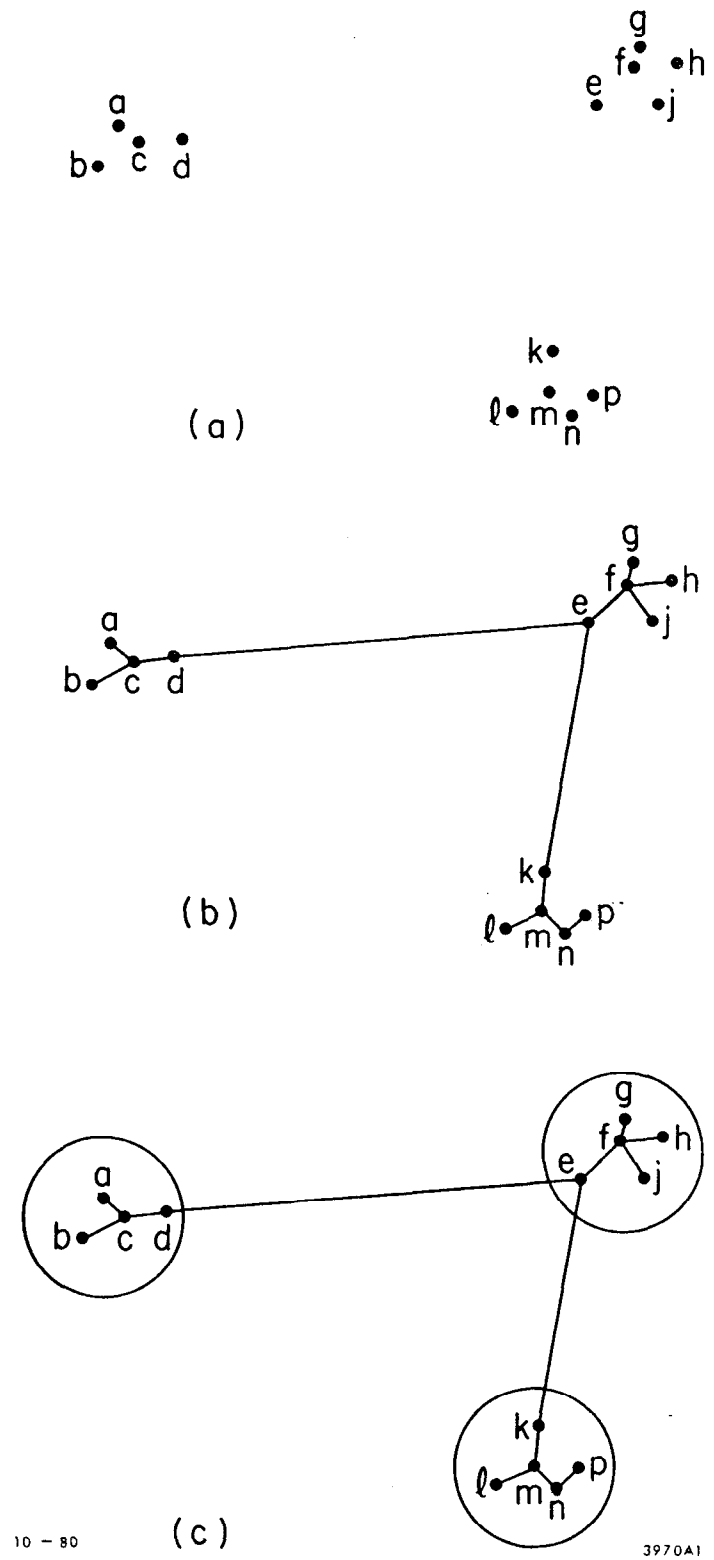

Fig. 7(a-c). A set of space points (nodes) are shown in (a) which are used to demonstrate the construction of a minimal spanning tree (b) and the partitioning of the minimal spanning tree into three clusters as indicated by the circles in (c). The partitioning occurs because the edges de and ek are long compared to the rest of the edge distances.

allows traversal from any space point to any other space point. Such a tree "spans" the space points. In addition we may select from the family of such spanning trees that one which has the shortest total length of interconnections. This defines the (unique) minimal spanning tree for the set of space points. Fig. 7(b) shows the minimal spanning tree for the space points in Fig. 7(a), assuming a two-dimensional Euclidean metric. The interconnections on the tree are henceforth called edges and there are two types of edges possible. An edge like de in Fig. 7(b) is termed bridging because removal of such an edge from the MST creates two subtrees. The edge bc however is nonbridging because if we remove it from the tree we do not create two subtrees, we merely isolate the node b. Hence the definition of clusters is trivial: remove all bridging edges which are larger than an (adjustable) parameter d_o. The parameter d_o should be chosen such as to be considerably longer than typical distances in the problem, distances like ac, bc, cd, etc. Hence with the single parameter d_o and the notion of an MST one can form clusters. Fig. 7(c) shows how a particular choice of d_o would lead to three clusters; the partitioning occurring because the bridging edges de and ek are considerably longer than the remaining tree edges. As a concrete physics example, imagine that the axes in Fig. 7 represent θ and ϕ and each node represents a particle in an e^+e^- hadron event. Fig. 7(c) thus represents a three-cluster (jet) event.

In practice the metric used to define the distance, d_{ij}, between particles i and j is given by

$$d_{ij} = \theta_{ij}^2 \; P_i^{-1} \; P_j^{-1}$$

where θ_{ij} is the angle between the two particles and P_i and P_j are the particle momenta. Ignoring the factor $P_i^{-1} P_j^{-1}$ for the moment, one sees that the factor θ_{ij} is the geodesic distance between particles i and j on the unit sphere. The second power of θ_{ij} is used because one is working on this two-dimensional surface. Hence θ_{ij}^2 takes into account the angular correlation. The addition of the inverse momentum weighting in d_{ij} is an attempt to include the effects of leading particles in jets. Small d_{ij}'s will result in clusters and the main effect of the inverse momentum weighting is to cluster soft particles around the leading particles.

So the procedure for finding clusters should now be clear. A selection of hadronic events is made. For each event, using the metric described above, a minimal spanning tree is constructed with the particles in the event as nodes in the tree. Bridging edges longer than d_o are removed thereby creating clusters. The vector momenta of the particles in the individual clusters are summed to generate cluster momenta. One final cut is made which requires that valid clusters have at least E_{min} energy. (The notion of a jet doesn't make sense for arbitrarily low jet energy.) The particles from clusters which do not pass the E_{min} cut are added back into the remaining clusters to which they are closest. Hence we see that only two parameters, d_o and E_{min}, suffice to generate the clusters. It should also be obvious, being free of any iterations, this MST method is extremely CPU efficient. The algorithm handles $\gtrsim 60$ hadronic annihilation events/sec. By contrast the MKII code for trijettiness and triplicity take $\gtrsim 1$ sec/event. Since d_o and E_{min} are parameters, how does one choose their value? The value for E_{min} is chosen by observing that at SPEAR, hadronic jets first become "visible" at

$E_{beam} \gtrsim 3$ GeV. Hence E_{min} should be chosen to be 3 GeV. In the MKII events used for the analysis below we typically observe only 70% of the energy hence E_{min} is lowered to 2 GeV for this reason. The parameter d_o is chosen so as to keep the contamination of produced two-jet events ($q\bar{q}$) from becoming more than 10% of the total of three-cluster events. We believe that in order to study the three-jet events one should not have sizeable backgrounds from $q\bar{q}$ events. Hence we use a Monte Carlo program to adjust d_o so that almost no ($< 2\%$) events produced as $q\bar{q}$ are classified as three-cluster events. The value of d_o used fo the analysis is $0.2\ (\text{GeV})^{-2}$.

The hadronic events used for this analysis are selected precisely as described in the previous section with one addition. Tracks in the endcap shower counters are used along with those in the barrel module shower counters. On average we see about 1.5 GeV/event in the endcaps. Five thousand events survive the cuts. The cluster frequency distribution resulting from the MST algorithm is shown for these data in Fig. 8, along with the results of the Monte Carlo simulated data.

In the spirit of the introduction of this chapter we have used the three-cluster (jet) events to look for evidence of gluons. Following the lead of the TASSO group[16] we have used the three-jet events to attempt to measure the spin of the gluon. Implicit in such a measurement is the assumption that the three-jet events are the result of gluon emission in $q\bar{q}$ events. The method used by the TASSO group and now the MKII was suggested by Ellis and Karliner[17] and involves using the measured jet energies to boost into the rest frame of the gluon and the quark (antiquark) which radiated it. Fig. 9 outlines the kinematics at the parton level. The quantities X_j are the jet energies (E_j) normalized to

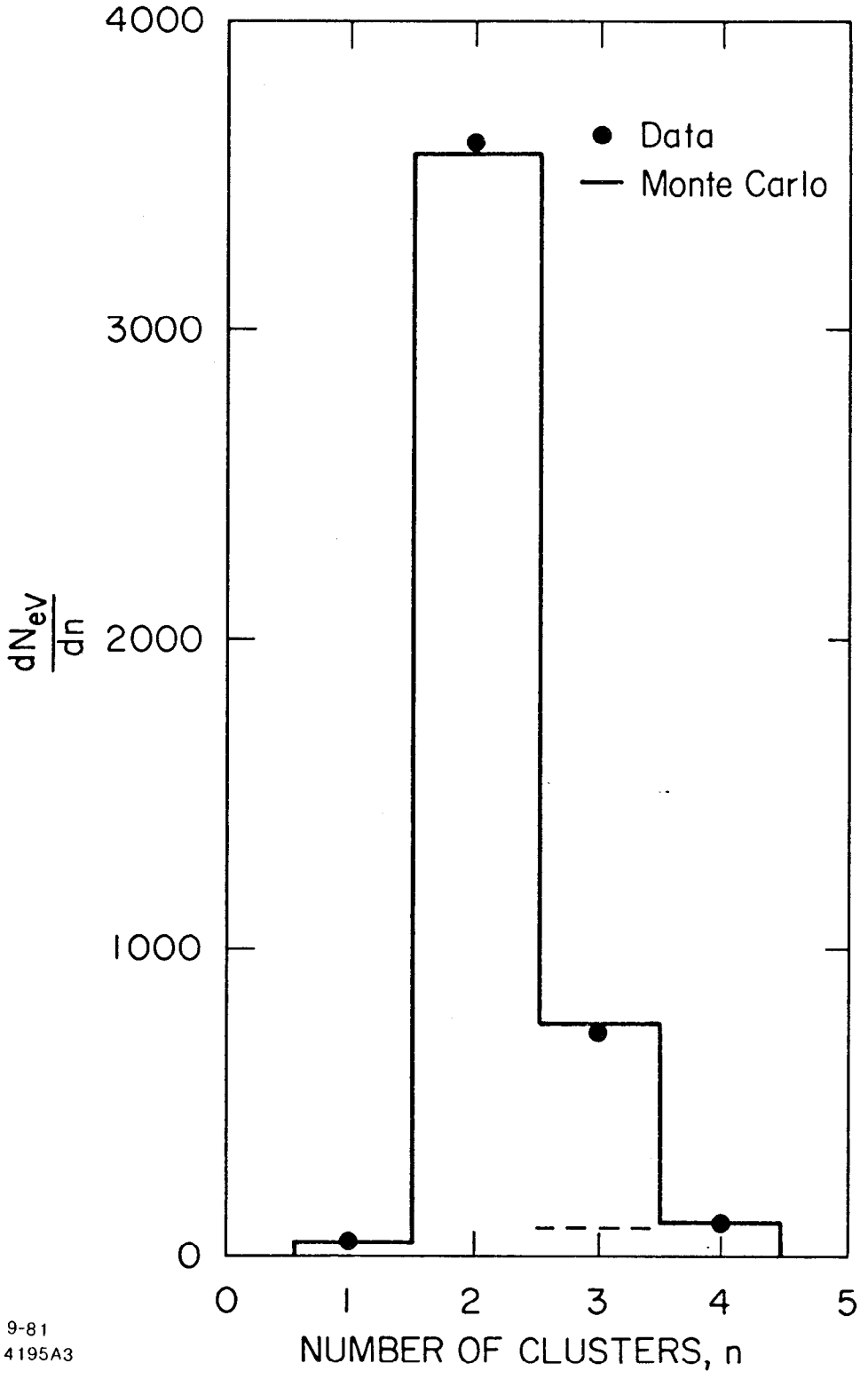

Fig. 8. The cluster frequency distribution for hadronic events is shown as solid dots and can be compared with the expectation of the Monte Carlo simulation program (solid curve). The majority of the events are classified as two-cluster events with a sizeable number of three-cluster events. The dashed line shows the number of three-cluster events which arise from Monte Carlo events generated as e^+e^- → quark-antiquark, i.e., two-jet events.

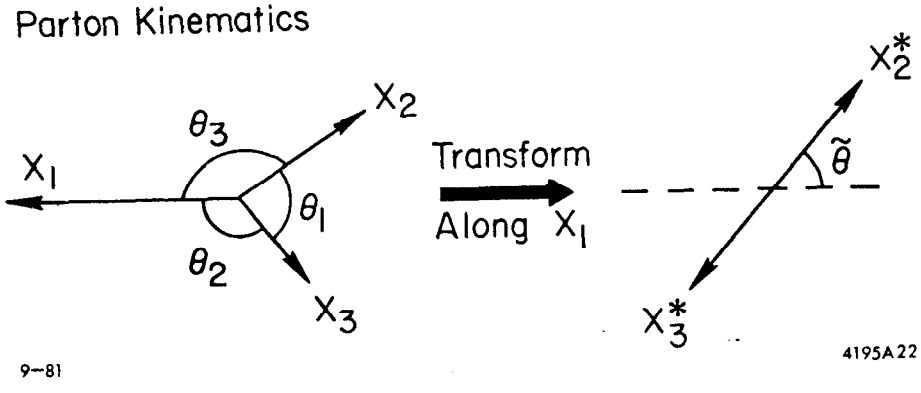

Fig. 9. This figure describes the parton kinematics for three-jet events. The variable x_1 ($x_j = E_j/E_{beam}$) is the thrust. For studying the spin of the gluon, we transform along x_1 into the rest frame of x_2 and x_3. $\tilde{\theta}$ is the production angle in this frame and $dN/d\cos\tilde{\theta}$ is sensitive to the gluon spin.

the beam energy: $X_j = 2E_j/E_{c.m.}$, j = 1, 2 and 3. The quantity X_1, referred to as the thrust, is the fractional energy of the highest energy parton. In the MKII detector jet directions are more precisely measured than jet angles but (in the limit of zero quark masses) knowledge of the jet directions and $E_{c.m.}$ permit the calculation of the X_j. One finds

$$X_j = \frac{2\sin\theta_j}{(\sin\theta_1 + \sin\theta_2 + \sin\theta_3)} \qquad (1)$$

where the angles θ_j are defined in Fig. 9. Boosting along the X_1 direction one arrives at the (X_2,X_3) center-of-mass. The production angle $(\tilde{\theta})$ of X_2 (or X_3) in this frame is given by

$$\cos\tilde{\theta} = \frac{X_2 - X_3}{X_1} = \frac{\sin\theta_2 - \sin\theta_3}{\sin\theta_1} \quad . \qquad (2)$$

Hence measurement of the jet directions (θ_j) allows for the calculation of $\cos\tilde{\theta}$. The presumption is that in most of the three-jet events ($\simeq$ 90%) X_2 or X_3 is the gluon and hence measuring the distribution of $\cos\tilde{\theta}$ is tantamount to sampling the gluon spin. Two hypotheses will be tested--namely that the gluon is a spin 1 or spin 0 object. The Ali et al. Monte Carlo used for this study has the option to select the $q\bar{q}g$ matrix element for the theoretically favored vector gluon or for the scalar gluon hypothesis.

It is important to realize (see Ref. 17) that the distribution $dN/d\cos\tilde{\theta}$ is a very strong function of the thrust, X_1. In addition, the X_1 dependence of $dN/d\cos\tilde{\theta}$ is quite different for the vector and scalar hypotheses. This coupled with the steep X_1 distribution, requires that the analysis be done with considerable care. In particular it is

important that the three-jet algorithm used have good thrust resolution. As we will see below the cluster algorithm has excellent X_1 resolution.

The three-cluster events are selected from Fig. 8 for the spin analysis. Because the parton kinematics in Fig. 9 is planar, we make a requirement that the three clusters be well defined in a plane (aplanarity results from particles which are not detected). Using the direction vector of clusters 1 and 2, we define a plane. Events are retained which have the angle between the direction vector of jet 3 and this plane less than 20°. Since $\cos(20^{\circ}) = 0.94$ the events so selected have very little momentum out of the event plane. We then use the jet directions to calculate the X_j according to (1). Fig. 10 shows the thrust distribution, dN/dX_1, so obtained with the prediction of the Monte Carlo events for the vector gluon hypothesis. The data are well simulated by the Monte Carlo program. The X_1 distribution for a scalar gluon is very similar to that of the vector gluon and Fig. 10 has insufficient accuracy to make a meaningful separation between the two hypotheses. Notice that we will only use events for which $X_1 \leq 0.9$. This cut is made because (a) it lessens the effects of fragmentation by demanding well separated jets and (b) the QCD calculations (theory) are shaky for $X_1 > 0.9$. The contamination of $q\bar{q}$ events in the three-jet sample is also lessened by this requirement. Using the vector gluon Monte Carlo simulation program we find that for the three-jet events selected above only 9% come from events produced as $q\bar{q}$. (This can be contrasted with the TASSO analysis which has 18% contamination.) We have studied the effect of these $q\bar{q}$ (mostly $b\bar{b}$) events on $dN/d\cos\tilde{\theta}$ and find that they populate the distribution uniformly. Again using the Monte Carlo simulation program we have studied how well the X_j's obtained from the jet directions agree with

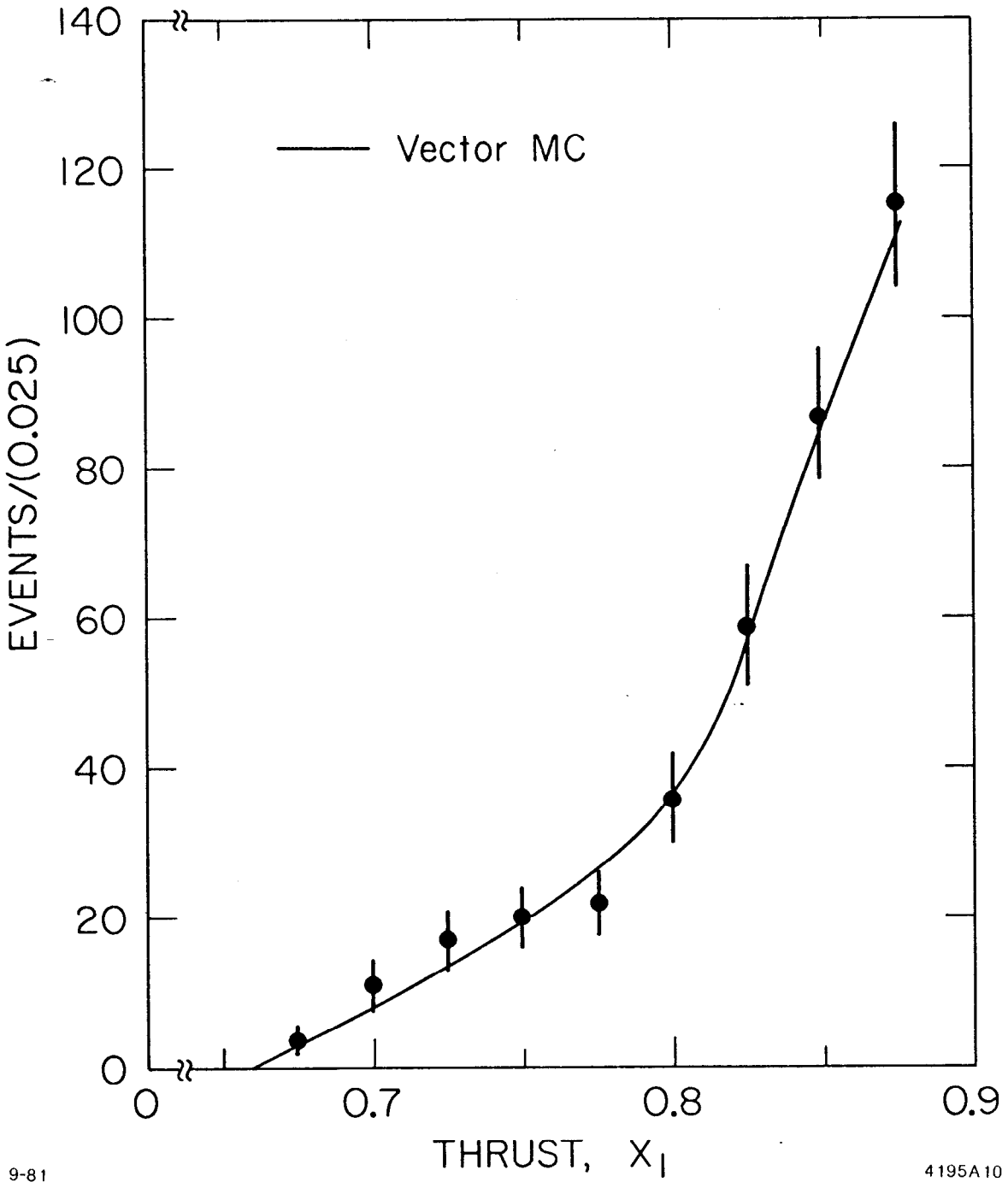

Fig. 10. The thrust distribution is shown for the three cluster events. The data and the Monte Carlo prediction are in good agreement. We restrict $x_1 < 0.9$ for reasons discussed in the text.

the produced parton energies. As an example, Fig. 11 shows the ratio of X_1 calculated from the jet angles to X_1 generated by the Monte Carlo. The distribution centers well around the value of one and has a width $\sigma_{X_1} \simeq 5\%$. Hence the thrust resolution obtained from application of the cluster algorithm is very good.

Using (2) we obtain $\cos\tilde{\theta}$ from the X_j's and Fig. 12 shows $dN/d\cos\tilde{\theta}$ for the data. Superimposed on the data are the results of the identical analysis on Monte Carlo events for both the vector and scalar gluon hypotheses. For this comparison the Monte Carlo distributions have been normalized to the number of data points. This caveat noted, it is seen that the vector model fits the data well, the scalar model less well. To remove the problem of the normalization, $\langle\cos\tilde{\theta}\rangle$ has been calculated for the data and the two Monte Carlo hypotheses. One finds that $\langle\cos\tilde{\theta}\rangle_{DATA} = 0.324 \pm 0.010$, $\langle\cos\tilde{\theta}\rangle_{VECTOR} = 0.314 \pm 0.007$ and $\langle\cos\tilde{\theta}\rangle_{SCALAR} = 0.290 \pm 0.005$. Hence the scalar gluon hypothesis is eliminated at about the 3σ level. This limit is about the same as that published by the TASSO group.[17] However at the recent Bonn Conference[18] additional data have strengthened the TASSO limit to a 5σ rejection of the scalar gluon hypotheses. TASSO uses the method of trijettiness for the study and it is comforting to see that two entirely different three-jet algorithms are arriving at the same conclusion.

Finally it was pointed out above that $dN/d\cos\tilde{\theta}$ is strongly thrust dependent. The MKII felt that the data should therefore be presented as a function of X_1. This is done in Fig. 13. (The results of the vector Monte Carlo are not shown because they are on top of the data.) Although more statistics are clearly needed, we can see that the thrust dependence of the data are different than that of the scalar gluon prediction.

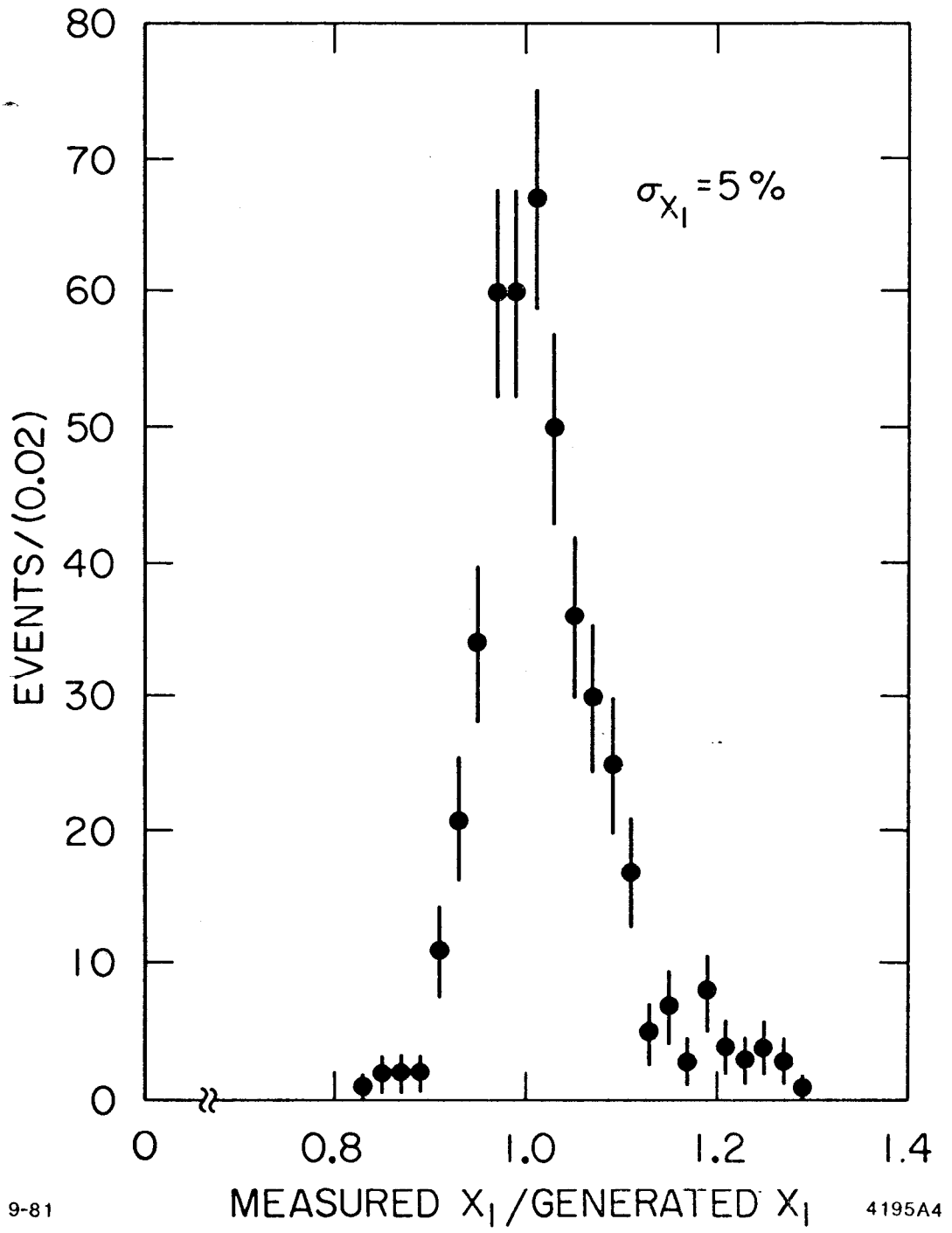

Fig. 11. This figure shows the resolution for x obtained from the three-cluster events used in the gluon spin determination. Since the thrust distribution is very steep (see Fig. 10) it is important to have good thrust resolution. The resolution obtained by comparing the measured thrust to the produced thrust in Monte Carlo events is 5%.

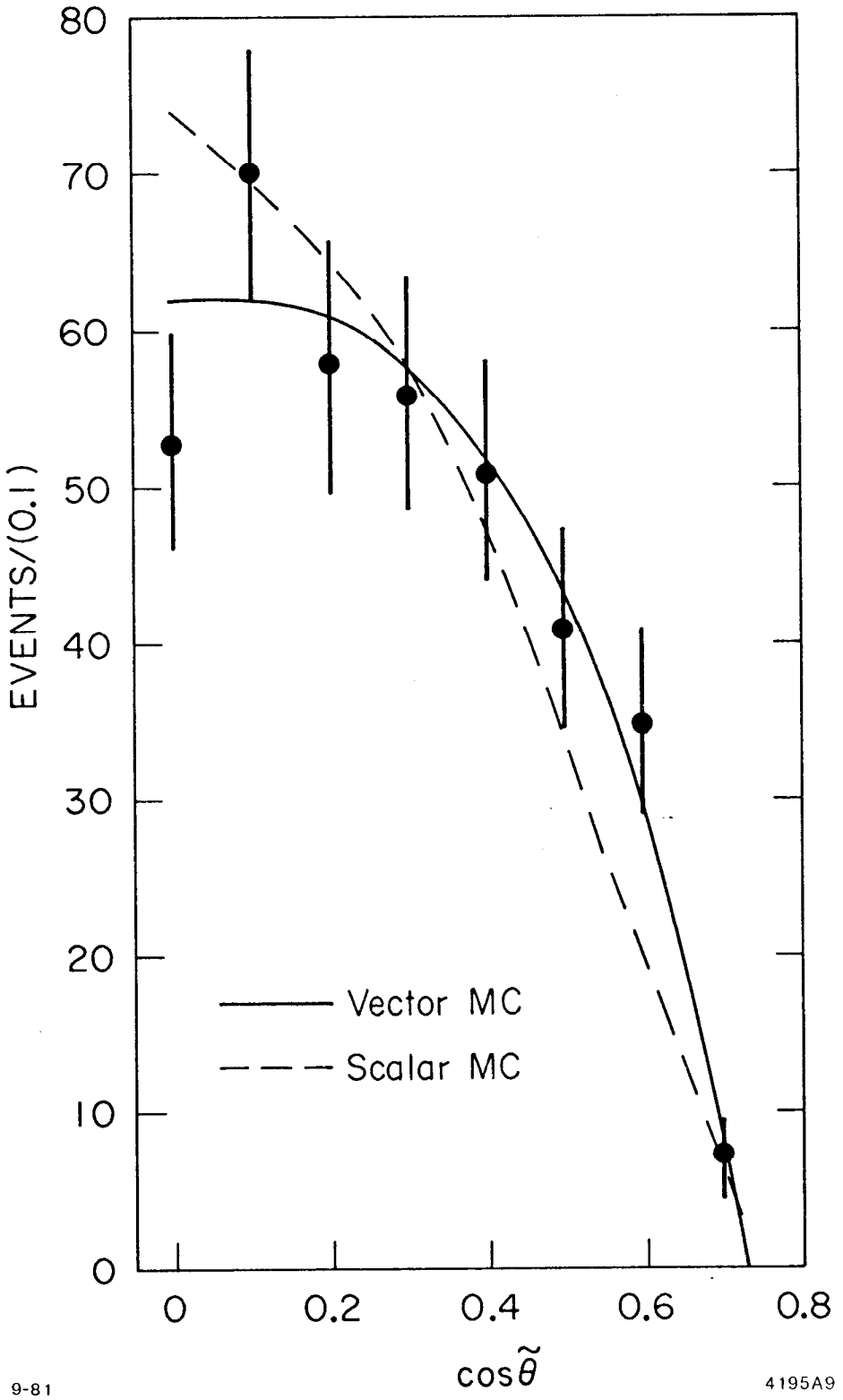

Fig. 12. This figure shows the distribution of cos$\tilde{\theta}$ for the data and the prediction of the Monte Carlo simulation program for vector and scalar gluons. The Monte Carlo predictions have been normalized to the data. The vector hypothesis is favored by the data.

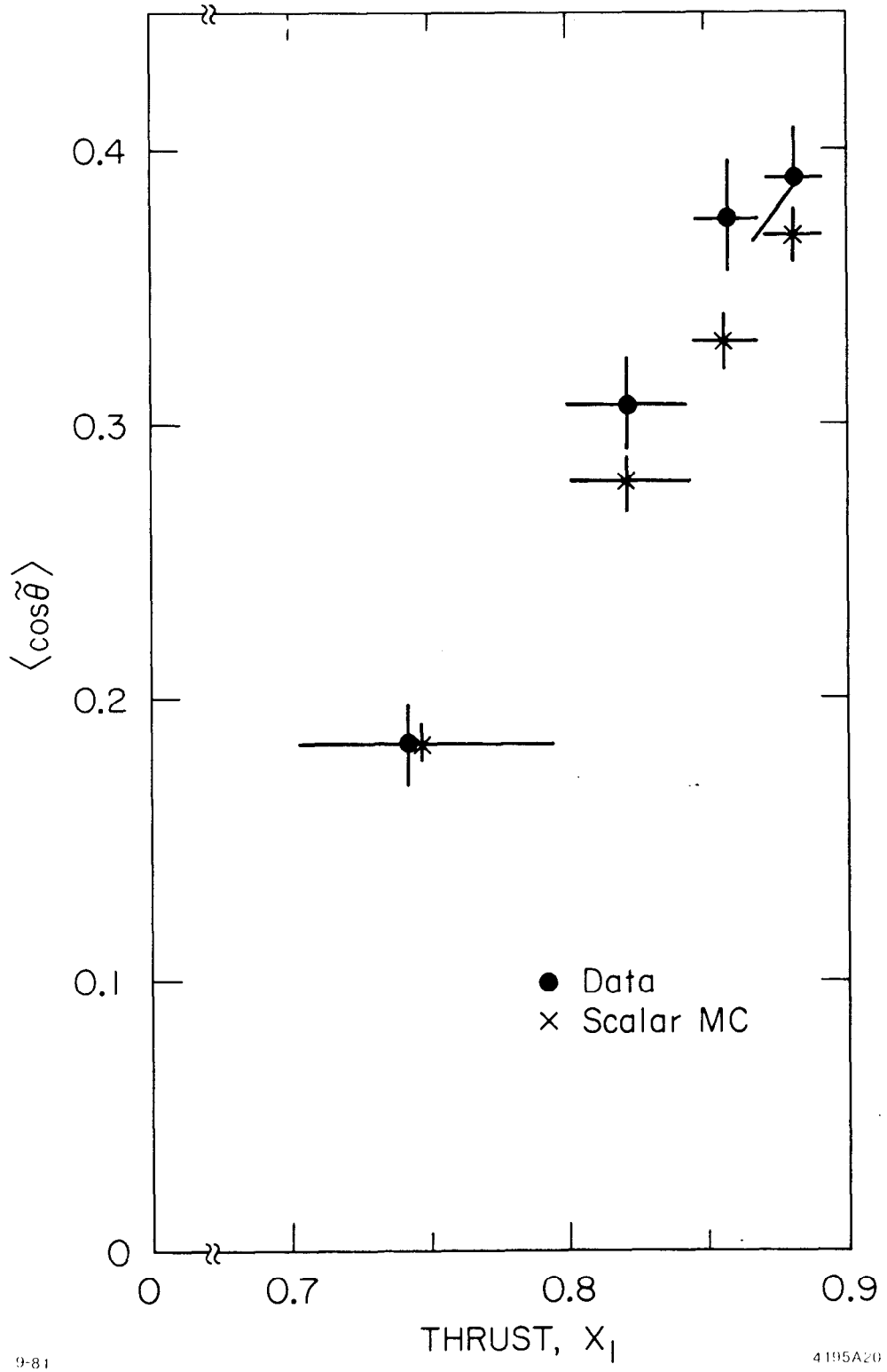

Fig. 13. $\langle \cos\tilde{\theta} \rangle$ is shown as a function of thrust for the data and the prediction of the scalar Monte Carlo. We see that, while more data are needed, the thrust dependence of $\langle \cos\tilde{\theta} \rangle$ for the data is different from that of the scalar Monte Carlo.

We have used the cluster algorithm to look into the question of whether the gluon fragments differently than the quark. The three-jet events are selected in exactly the same way as for the gluon spin measurement. Using the calculated X_j's, the jets are ordered according to X or equivalently according to their energy ($E_j = X_j E_{c.m.}/2$). Using the particles assigned to the jets by the cluster algorithm, we obtain the distribution of the particle transverse momentum ($P_\perp$) relative to the jet direction. This is done for each jet separately. Figure 14 shows the $dN/dP_\perp$ distributions for the highest energy jet, the intermediate energy jet and the lowest energy jet. The average jet energies for these three categories are 3.9 GeV, 8.3 GeV and 14.1 GeV, respectively. It should be further noted that the lowest energy jet can be associated with the gluon 51% of the time. From Fig. 14 we calculate that $\langle P_\perp \rangle$ for the highest energy jet, the intermediate energy jet and the lowest energy jet are 0.372 ± 0.010 GeV/c, 0.343 ± 0.010 GeV/c and 0.317 ± 0.010 GeV/c, respectively. This confirms the now familiar PETRA result of jet broadening with increasing jet energy. This broadening is well accounted for by the gluon bremsstrahlung simulations. Also shown in Fig. 14 as a solid line is the result for $dN/dP_\perp$ obtained by the MKI group[19] for quark jets at SPEAR. These data come from the MKI running at $E_{c.m.} = 7.0$-7.4 GeV and hence correspond to an average jet energy of 3.6 GeV. All distributions in Fig. 14 are for detected events only; no corrections have been applied for the detector biases. For this reason we have adjusted the vertical scale of the MKI data such that the curve best represents the MKII PEP low energy jet distribution. One sees from the comparison that for jets of comparable energies the PEP jets, which are 50% gluon rich, appear to have the same transverse fragmentation as the quark jets.

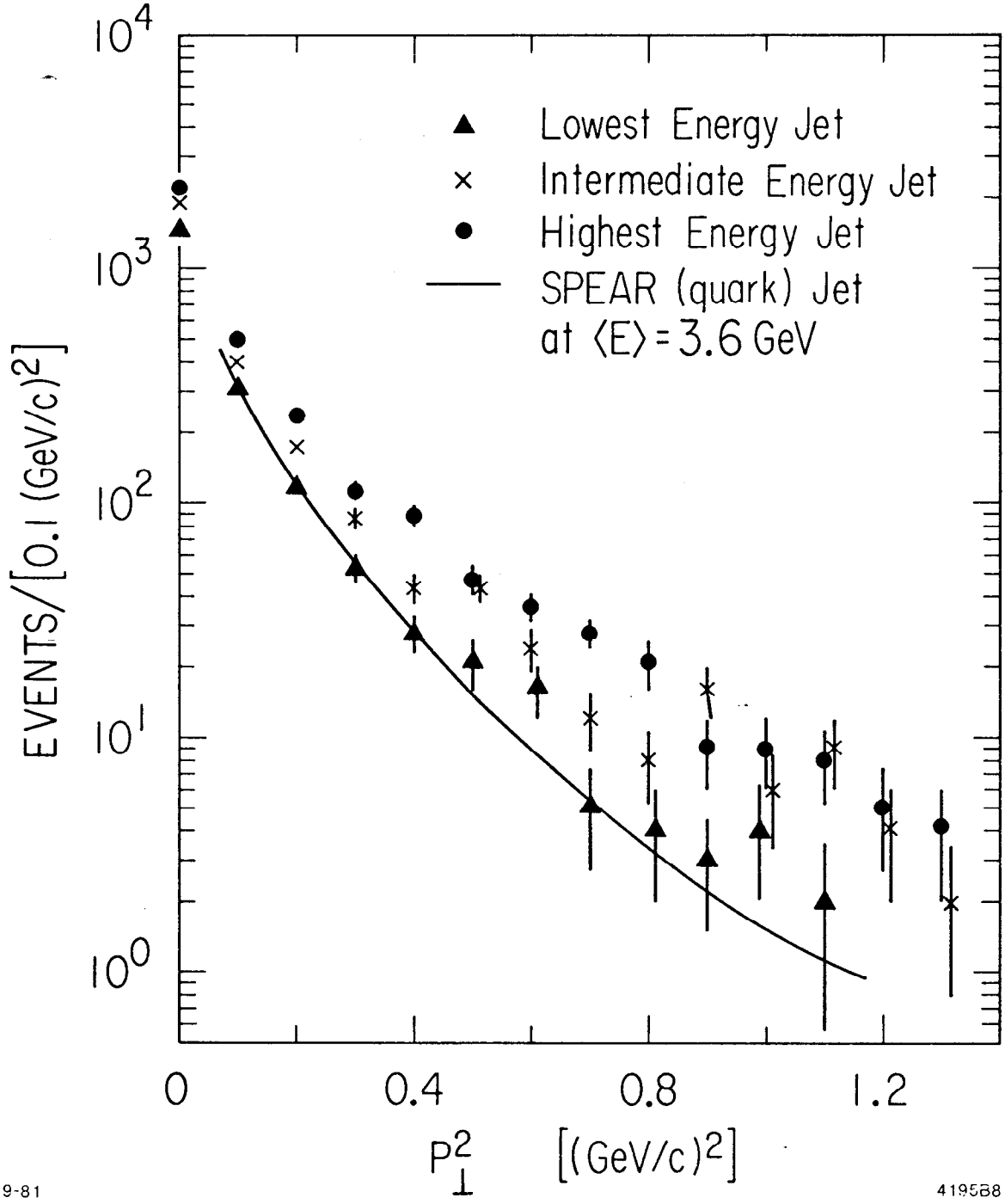

Fig. 14. The transverse momentum structure of the three individual jets in the three-cluster events is shown. The jets have been ordered by their energy. We clearly see the effect of jet broadening with increased jet energy which results from the gluon bremsstrahlung. The low-energy jet ($\langle E \rangle$ = 3.9 GeV), which is expected to contain about 50% gluons, is compared with a quark jet ($\langle E \rangle$ = 3.6 GeV) from MKI SPEAR data (solid line). The low energy PEP jet has $\langle P_\perp \rangle$ = 317 MeV/c and that of the quark jets 310 MeV/c. Hence for energies in the 3-4 GeV range it appears that quarks and gluons have a similar transverse fragmentation behavior.

The $\langle P_\perp \rangle$ for the SPEAR quark jets is $\langle P_\perp \rangle = 0.310 \pm 0.010$ in good agreement with $\langle P_\perp \rangle = 0.317 \pm 0.010$ for the PEP lowest energy jet.

ENERGY-ENERGY CORRELATIONS

It is desirable to perform tests of QCD which are not strongly dependent on Monte Carlo simulations which, in themselves, embody QCD. Tests performed in which the detected data are compared with the Monte Carlo predictions can depend very strongly on the models used in the Monte Carlo programs. It is preferable to perform tests on quantities that can be calculated in the framework of QCD and can be measured directly in an experiment which requires only small corrections for detector biases. In this way the data stand on their own and, should the theoretical predictions change (higher orders are included), valid comparisons are still possible with the data. Among such quantities the energy-energy correlation is particularly interesting because it does not require the selection of specific event topologies, such as three-jet events, nor does it depend on the definition of a jet axis.

The MKII group has made a high statistics study[20] of the energy-energy correlation in the PEP hadronic events. This method looks at energy flow by considering the correlations in energy between particle pairs. We can define an energy weighted cross section for observing the energy E in the phase space element $d\Omega$ and E' in $d\Omega'$ as

$$\frac{1}{\sigma_o} \frac{d\Sigma}{d\Omega d\Omega'} = \frac{1}{N} \sum_N \sum_{\text{pairs}} \frac{E}{\sqrt{s}} \frac{E'}{\sqrt{s}} f \qquad (3)$$

The first sum ranges over the total number of events (N), the second over all pairs of particles in the phase space elements $d\Omega$ and $d\Omega'$. The statistical factor f is two for pairs of different particles, one for

self-correlations. The total hadronic cross section is denoted σ_o and $\sqrt{s} = E_{c.m.}$. For the sake of further discussion we define χ to be the angle between the direction vector of the two particles entering the calculation of the cross section.

The cross section defined for hadrons in (3) has been calculated[21] for partons in the framework of first order perturbative QCD. The form of the cross section for partons is

$$\frac{1}{\sigma_o}\frac{d\Sigma}{d\Omega d\Omega'} = \frac{3\alpha_s}{16\pi}\left[A(\chi,\alpha_s)(2+\cos^2\theta+\cos^2\theta') + B(\chi,\alpha_s)(\cos\chi+\cos\theta\cos\theta')\right] \quad (4)$$

The functions A and B depend on only one angle, χ, and have been calculated to first order in α_s. They both vary linearly with α_s. The function A describes the correlation between a quark and an antiquark; B describes the correlation between a quark (antiquark) and a gluon. In each case the partons are characterized by the polar angles θ and θ' and the angle between them is χ. The explicit forms of A and B add little insight to this discussion and can be found in Ref. 21.

In order to make a meaningful comparison between the experimental cross section for hadrons, (3), and the theoretical prediction for partons, (4), we must account for the nonperturbative effects of fragmentation. This has the effect of augmenting the term A above. It has been calculated[22] that this function has the form

$$A_{qf}(\chi) = \frac{C\langle P_\perp\rangle}{\sqrt{s}\,\sin^3\chi} \quad .$$

Here $\langle P_\perp\rangle \simeq .3$ GeV characterizes the average transverse momentum in the hadronization and C is a constant (~ 4) which is a measure of the "density" of hadrons in the fragmentation process. It is important to

notice that A_{qf} is symmetric about $\chi = \pi/2$. This is expected since it arises from the symmetric two-jet final state. The first order perturbative cross section (4) has a singularity at $\chi = \pi$ which corresponds to a quark and antiquark becoming collinear with a soft gluon. There is a weaker singularity at $\chi = 0$ when a quark (antiquark) becomes collinear with a hard gluon. In the intermediate angular range ($30^{o} < \chi < 150^{o}$), where one is not dealing with correlations in the center of the jets, there is a pronounced asymmetry about $\chi = \pi/2$. This serves to distinguish the perturbative and nonperturbative contributions to the energy correlation.

The event selection for this analysis is identical to that described earlier with the exception that the events so selected are required to have at least one particle in the fiducial volume defined by $-0.7 < \cos\theta < 0.7$. 3200 events pass the selection criteria.

The cross section (3) can be presented in an integral form where we sum over all external particle directions keeping the angle χ fixed. This yields the following cross section

$$\frac{1}{\sigma_o}\frac{d\Sigma}{d\cos\chi} = \frac{1}{\Delta\chi\,\cos\chi\,N}\sum_{N}\sum_{\text{pairs}}\frac{EE'}{s}\,f\ .$$

This cross section for the MKII fiducial volume is shown in Fig. 15. Corrections have been applied for the effects of resolution, detector inefficiencies, initial state radiation and weak decays. These corrections are modest--20% for $\chi = 30^{o}$ dropping to 5% for $\chi = 90^{o}$. We see, in Fig. 15, the fact that most particles are confined to two jets. There is a strong peaking at $\chi = 0$ (particles in the same jet) and $\chi = \pi$ (particles in opposite jets). Also shown in Fig. 15 is Eq. (4)

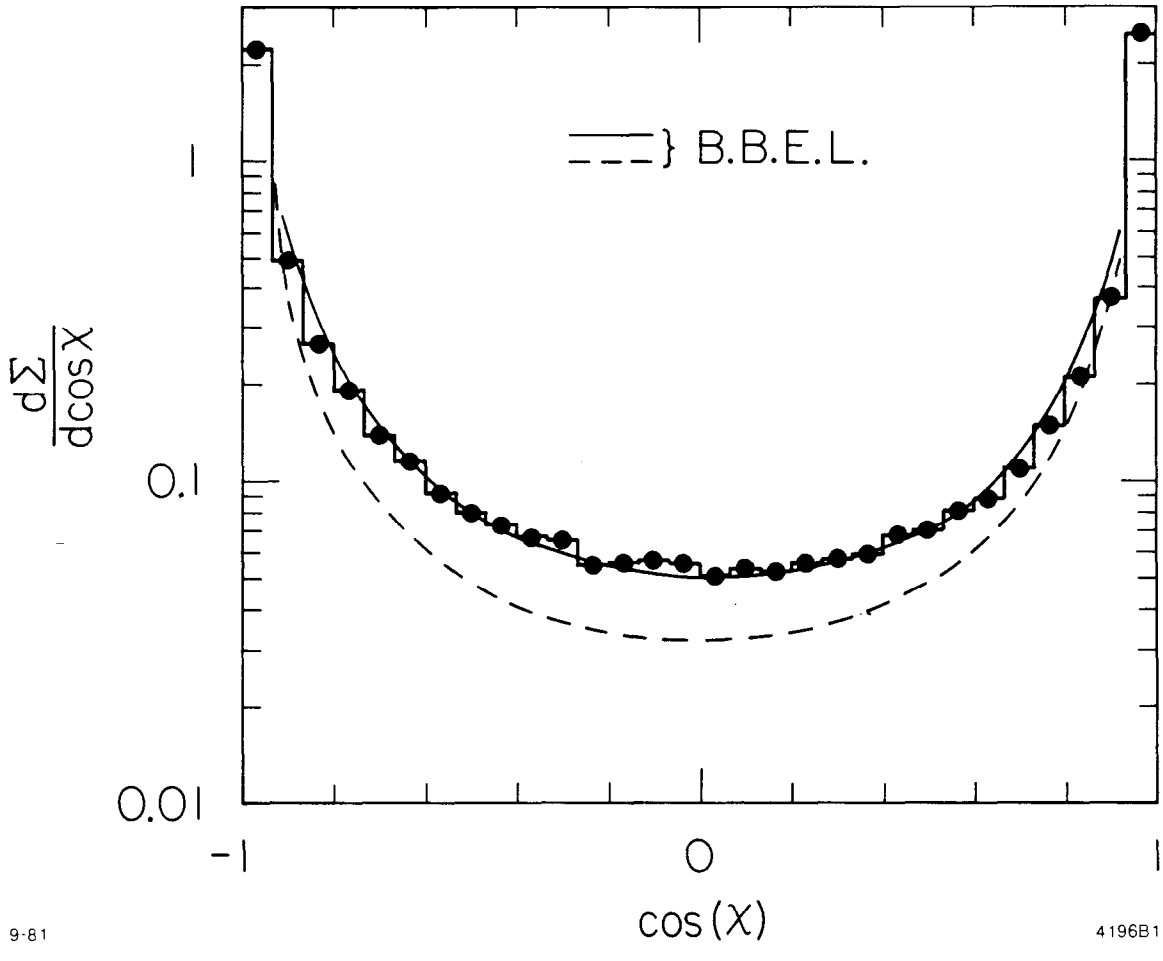

Fig. 15. This figure shows $(1/\sigma_0)\ d\Sigma/d\cos\chi$ as a function of $\cos\chi$. The size of the dots correspond to statistical errors in the data points. The solid line is the QCD prediction of Basham, Brown, Ellis and Love including the nonperturbative contribution. The broken line is the nonperturbative part alone ($\alpha_s = 0$).

integrated over the MKII fiducial volume. This QCD prediction, including the effects of fragmentation, reproduce the data very well.

However as a more valid test of QCD we will consider the asymmetry defined as

$$D(\chi) = \frac{d\Sigma}{d\cos\chi}\ (\pi-\chi) - \frac{d\Sigma}{d\cos\chi}\ (\chi) \quad .$$

Remembering what was said earlier about A_{qf}, this measure of QCD is much less dependent on the effects of fragmentation which, being symmetric about $\chi = \pi/2$, cancel in $D(\chi)$. The measurement of $D(\chi)$ is given in Fig. 16. Notice that D changes by about two orders of magnitude in going from $\chi = 30^{\circ}$ to $\chi = 90^{\circ}$. The shape of $D(\chi)$ is predicted absolutely by QCD and the magnitude is proportional, in first order, to α_s. A single parameter fit to the data yields

$$\alpha_s = 0.180 \pm 0.015 \pm 0.020$$

with a χ^2 of eight for nine degrees of freedom. The two errors quoted are statistical and systematic, respectively; the systematic error arises from assuming that there is a 20% uncertainty in the Monte Carlo corrections. We wish to emphasize that α_s obtained from this comparison of QCD with the data must be interpreted within the constraints of the theoretical calculations. One obvious constraint is that it is a first order calculation. In reality α_s is a parameter in the theoretical calculation and if, for instance, second order effects are large, this parameter obtained above may be substantially different from the strength of the true strong coupling constant.

The energy-energy correlation has been measured by the PLUTO group at PETRA.[23] Because of limited statistics, the PLUTO group cannot obtain

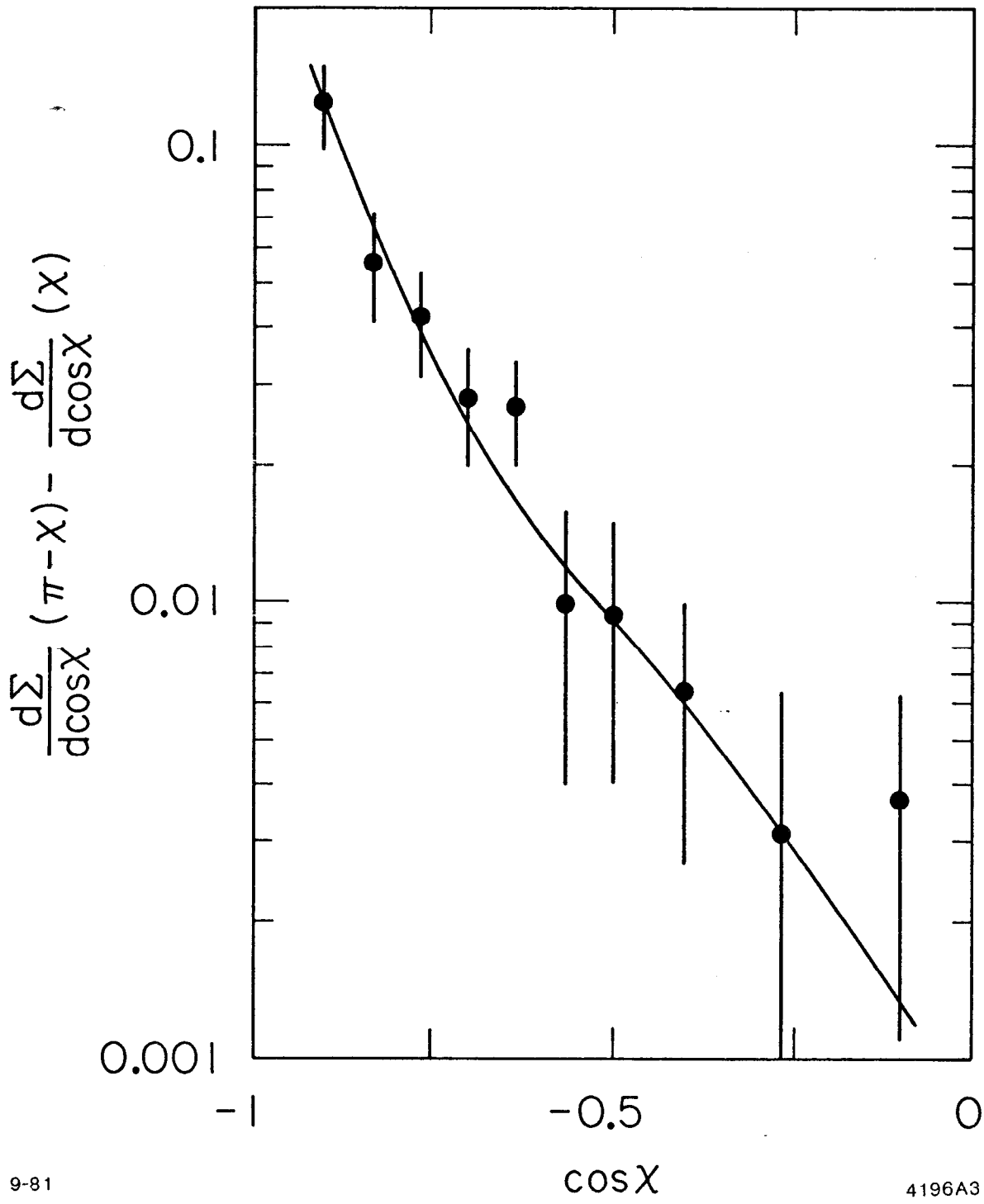

Fig. 16. The asymmetry, $D(\chi)$, is shown as a function of $\cos\chi$. The solid line is the QCD prediction with $\alpha_s = 0.18$.

α_s from the asymmetry. Rather they obtain $\alpha_s = 0.2 \pm 0.02$ from a fit to the full energy correlation function (i.e., as in Fig. 15).

MEASUREMENT OF THE τ LIFETIME

A measurement of the τ lifetime provides a direct determination of the strength of the coupling of the τ to the charged weak current. In the standard model this coupling strength would be the same as the muon and a simple calculation yields

$$t_\tau = \left(\frac{M_\mu}{M_\tau}\right)^5 t_\mu B_e = (2.8 \pm 0.2) \times 10^{-13} \text{ sec} .$$

Here the symbols t and M stand for the lifetime and mass, respectively, and B_e is the τ branching fraction[24] for the decay $\tau^- \to e^- \bar{\nu}_e \nu_\tau$. The error on the numerical value of t_τ comes almost entirely from the error in B_e. For $E_\tau = E_{c.m.}/2 = 14.5$ GeV the mean τ flight path, ℓ_τ, is 700 μ. We have made a measurement of ℓ_τ using a resolution $\delta(\ell_\tau) = (3\text{-}4)$ mm. This has been achieved by controlling the systematic error to 300 μ and beating the resolution problem with statistics.

To measure the τ lifetime we located the vertex of three-prong decays and calculated the flight distance between the center of the luminous spot and the vertex projected along the τ momentum. The decay results from the production process

$$e^+e^- \to \tau^+\tau^- \qquad (5)$$

in which we have selected events to have either one or both of the τ's decay to three-charged particles (plus any number of π^0's). Hence events were selected which had four or six charged particles. The plane perpendicular to the sphericity axes was then used to partition the event into two jets; at least one of the jets was required to contain three particles with net charge of ±1.

There are four sources of background: beam gas events, two-photon production of τ's ($e^+e^- \to e^+e^-\tau^+\tau^-$), $e^+e^- \to$ hadrons and radiative Bhabha events in which the radiated photon undergoes a conversion ($e^+e^- \to e^+e^-\gamma \to e^+e^-e^+e^-$). Beam gas events and two photon production result in a small amount of visible energy and these backgrounds are removed by requiring either at least 0.25 $E_{c.m.}$ in visible, measured energy or at least 0.125 $E_{c.m.}$ visible energy accompanied by either a muon or a lepton. Hadronic events are removed by requiring a small ($\lesssim 1.89$ GeV/c^2) jet invariant mass. Radiative Bhabhas are removed by requiring that the invariant mass of the three-prong jet, assuming each particle to be an electron, be greater than 0.3 GeV/c^2. In addition we required that the total energy measured by either the tracking system or the liquid argon calorimeters be less than 0.9 $E_{c.m.}$.

The data set analyzed contains the full 15.4 pb^{-1} statistics and corresponds to about 1500 produced $\tau^+\tau^-$ pairs. The selection cuts described above isolate 284 events containing 306 three-prong decay vertices. The kinematics and rate of these events are entirely consistent with the production process (5). We now treat each three-prong decay as a separate event. In order to reduce the (sizeable) effects of scattering or mismeasurement, quality cuts were made on the charged tracks. These include requiring signals from at least ten of the drift chamber layers, a good fit to the trajectory and a momentum of at least 500 MeV/c. These cuts left 126 three-prong decays.

We now found the intersection point of the three-tracks by varying the track trajectory parameters within their measured errors using a least squares minimization. Using the χ^2 obtained from this vertex finding procedure, we eliminated eight events ($\chi^2 > 15/3DOF$). The error

in the vertex position projected along the τ flight direction is shown in Fig. 17. (In reality the vertex finding is done in the plane perpendicular to the direction of the incident e^+ and e^- beams. The two dimensional vertex position and error are then converted to three dimensions using the τ direction vector.) From Fig. 17 we see that the vertex position resolution is of the order of (3-4) mm. For future manipulation the data are divided up into two sets; those events which have a vertex error of < 4 mm and those which have a vertex error between 4 and 8 mm. There are sixteen events with vertex errors above 8 mm. These are eliminated since they contain very little information about the τ lifetime.

Having found the three-prong vertex, the τ flight path is calculated as the distance between the vertex and the luminous spot projected onto the τ momentum vector. The position of the luminous spot was obtained by measuring the crossing point of the electron and positron in Bhabha events. The data were divided up into many blocks of consecutive runs and we found that over these blocks of runs the beam crossing position was very stable. The vertical and horizontal size of the luminous spot, corrected for measurement resolution, was found to agree very well with the known PEP beam size.

Figure 18 shows the τ flight distance for (a) all the data and (b) for those events with a vertex resolution of < 4 mm. A clear positive lifetime is evident in this figure. In Fig. 18(a) there are 35 events with negative flight paths and 67 with positive flight paths; the probability of this occurring for a τ of zero lifetime is 0.2%.

A maximum likelihood fit was performed to the distributions in Fig. 18 to obtain the most probable mean flight path for the τ. Entering the fit was the flight distance spectrum obtained from a

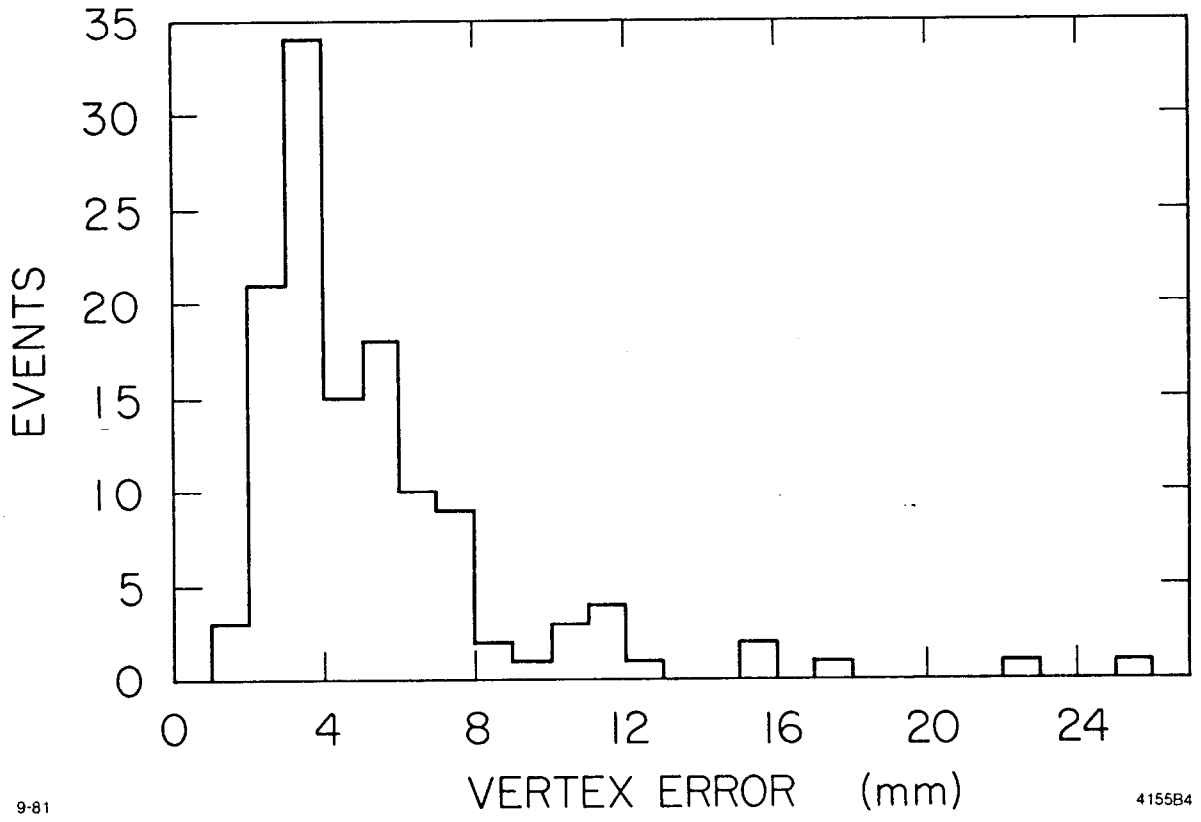

Fig. 17. The vertex error for three-prong τ decays is shown. Typical errors are 3-4 mm.

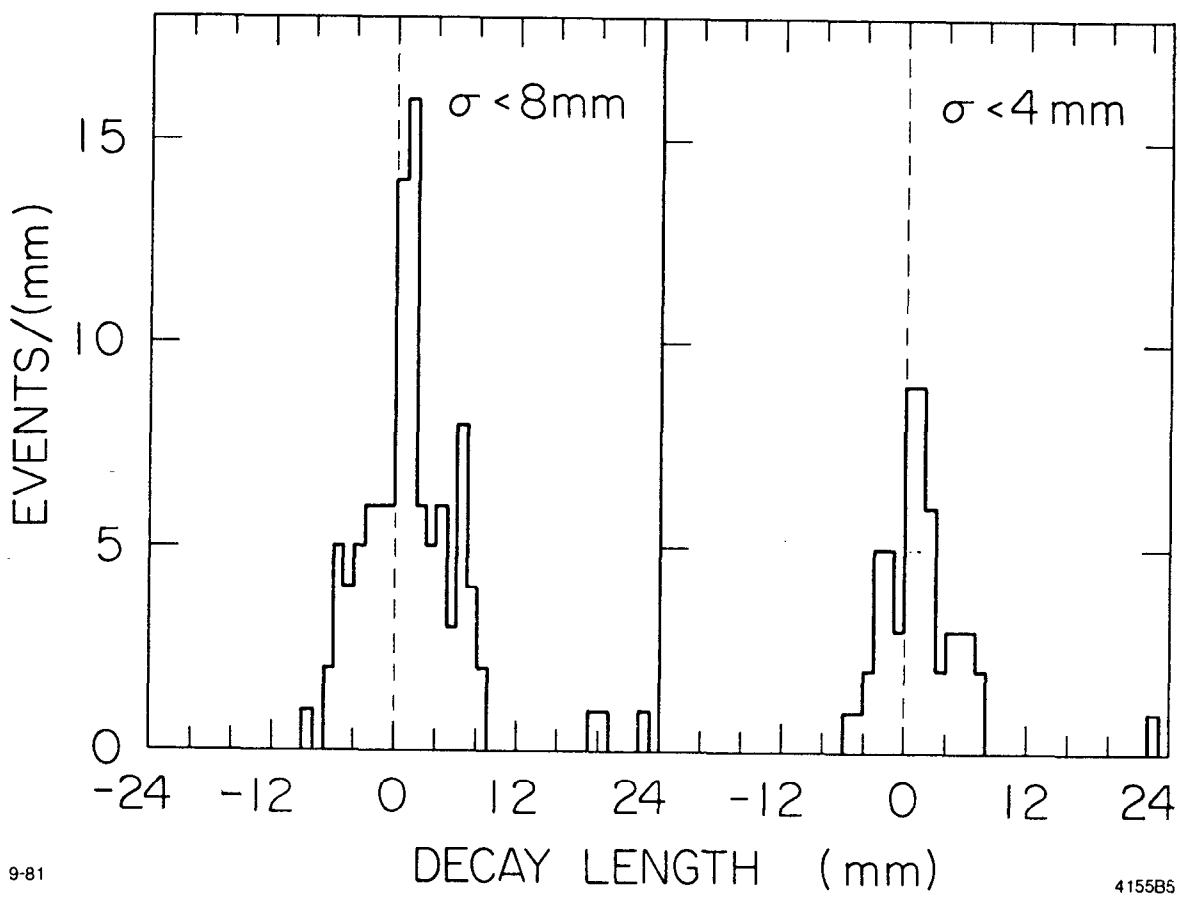

Fig, 18. This figure shows the τ decay length distribution for events with vertex resolution < 8 mm (a) and < 4 mm (b). An excess of positive decay lengths events is seen.

Monte Carlo simulation with a zero τ lifetime convoluted with an exponential decay distribution. As with all the analyses presented in this talk, the Monte Carlo simulation program generated raw data which were then run through the identical analysis programs as the real data. The two resolution bins were fit simultaneously for a common mean flight distance. The result obtained is $\ell_\tau = (1.07 \pm 0.37)$ mm where the error only reflects the statistics.

A careful study of systematic effects in either the detector or the analysis procedure was undertaken. Many sources of systematic error are eliminated because of the cylindrical symmetry of the detector. Almost all effects tend to worsen the vertex resolution but do not create a net positive flight path. An example of such an effect would be a shift in the position of the luminous spot. To check for biases in the analysis programs, Monte Carlo simulations for the expected τ lifetime and a lifetime four times that expected were performed. In both cases the result of the analysis agreed with the input lifetime within the statistical errors. A test of the Monte Carlo simulation was performed using multihadron events. Fake three-prong τ decays were created by selecting the three most energetic tracks within a jet and analyzing them as if they came from a τ decay. A mean flight distance of (0.45 ± 0.11) mm was obtained for the real data which should be compared with the result from a Monte Carlo simulation of (0.34 ± 0.11) mm. When the Monte Carlo simulation was run with zero K_S^o and D lifetimes, the resulting mean flight path was (0.11 ± 0.13) mm. These results indicate that the Monte Carlo simulates the measured data to within $\lesssim 0.2$ mm and that a substantial fraction (if not all) of the positive mean flight distance in the multihadronic events is from K_S^o and D decays. As a result of all the

above checks, and others not mentioned, we have estimated the systematic uncertainty in the τ mean flight path to be $\lesssim 0.3$ mm. Backgrounds have been studied either from the data or by Monte Carlo simulations and are estimated to contribute 7.5 events to the data sample. The mean flight path for the τ has been corrected up by 4% for the presence of these events.

The final result of this analysis, combining the statistical and systematic errors in quadrature, is

$$t_\tau = (4.6 \pm 1.9) \times 10^{-13} \text{ sec} .$$

Comparing this with the theoretical expectation quoted earlier we see that, within one standard deviation, the τ coupling to the weak charged current is 0.66 to 1.02 times that expected from τ-μ universality. This MKII measurement constitutes the first evidence of a positive flight path in τ decays. However, the TASSO group presented the results of their τ lifetime measurement in Bonn. Based on a flight path distribution which has a negative mean, they obtain a result of

$$t_\tau = (-0.25 \pm 3.5) \times 10^{-13} \text{ sec} .$$

This corresponds to a 95% confidence upper limit of 5.7×10^{-13} sec.

STUDY OF EVENTS OF THE TYPE $e^+e^- \to e^\pm\mu^\mp$

The $e\mu$ final state proved very powerful as an analytic tool at SPEAR and led to the discovery of the heavy lepton. Since we now know a lot about the heavy lepton and have sound measurements of all of its major decay branching fractions, it is possible to look for $e\mu$ event signals at PEP -- signals above and beyond those from $e^+e^- \to \tau^+\tau^-$. In particular, we may search for a yet heavier lepton. Such heavy leptons have been

looked for at PETRA.[25] All these searches use the multibody hadronic decay modes of the τ and hence require detailed models of such decays for the new heavy lepton. We are the first group to use the $e\mu$ events which have the advantage of both a simple analysis and a simple model for the heavy lepton leptonic branching fraction. Also from the $e\mu$ events we will obtain limits on the production and decay to $e\nu$ and $\mu\nu$ of point, spin 0 bosons.

All of the 15.4 pb^{-1} data sample was used for this analysis. Events were selected to have two oppositely charged particles, one of which was identified as an electron by the liquid argon shower counters and the other as a muon. Both tracks are required to have momenta > 1.5 GeV/c. The misidentification of pions as electrons has been measured at PEP to be $\lesssim 1\%$ for momenta above 1 GeV/c. The muons are required to penetrate at least 21" of steel; the corresponding pion misidentification probability is $\lesssim 1\%$. The events are also required to have no photons, except within 10^{o} of the electron. The 10^{o} cut allows events in which the electron radiates to enter the analysis.

Twenty-five events survive the above cuts; the Monte Carlo simulation program, including 0.3 events from two-photon production of τ's, predicts 23.5 ± 3.3 events. Hence the $e\mu$ events seen are consistent in number with coming entirely from conventional τ production.

To search for high mass leptons we use the correlation between a particle's mass and the transverse momentum imparted to its decay products. The variable $P_\perp$ is defined by

$$P_\perp = \frac{|(P_e \times P_\mu) \cdot \hat{k}|}{|(P_e - P_\mu) \times \hat{k}|}$$

where $\hat{k}$ is the unit vector in the direction of the e^+ beam (z). In words we define $P_\perp$ by finding an axis such that the momenta of the e and μ transverse to the axis, and projected into the xy plane, are equal. The data as a function of $P_\perp$ are shown in Fig. 19 along with the absolutely normalized distribution expected for τ decays. Clearly the τ decays account very well for the data. The presence of a new heavy lepton would add events to Fig. 19--the higher the mass of the new lepton the larger the mean contribution to Fig. 20. For the sake of comparison, the effect of a 10 GeV/c^2 heavy lepton is shown on Fig. 19, where the normalization is obtained from a simple model discussed below. The data in Fig. 19 have been fit for the presence, in addition to the τ, of a new heavy lepton. The sole parameter in the fit is the leptonic branching fraction of the new heavy lepton. The resulting 95% confidence level upper limits on $(B_e B_\mu)^{1/2}$ are given in Fig. 20. The curve rises quickly as one approaches masses of the order of the beam energy because of the production cross section threshold behavior.

In order to interpret the results of Fig. 20, we need a model for the leptonic branching fraction of the heavy lepton. In the assumed model, the hadronic part of the decay is calculated as if quarks were free particles. Then the three leptonic branching fractions (B_e, B_μ and B_τ) are

$$B_\ell \propto (1 - 8y + 8y^3 - y^4 - 12y^3 \ln y)$$

where $y = M_\ell^2/M^2$ and $M(M_\ell)$ is the mass of the heavy lepton (lepton). The two hadronic branching fractions (B_{ud} and B_{cs}) are given by

$$B_h \propto 3\left(1 + \frac{\alpha_s}{\pi}\right) (1 - 8y + 8y^3 - y^4 - 12y^2 \ln y) \quad .$$

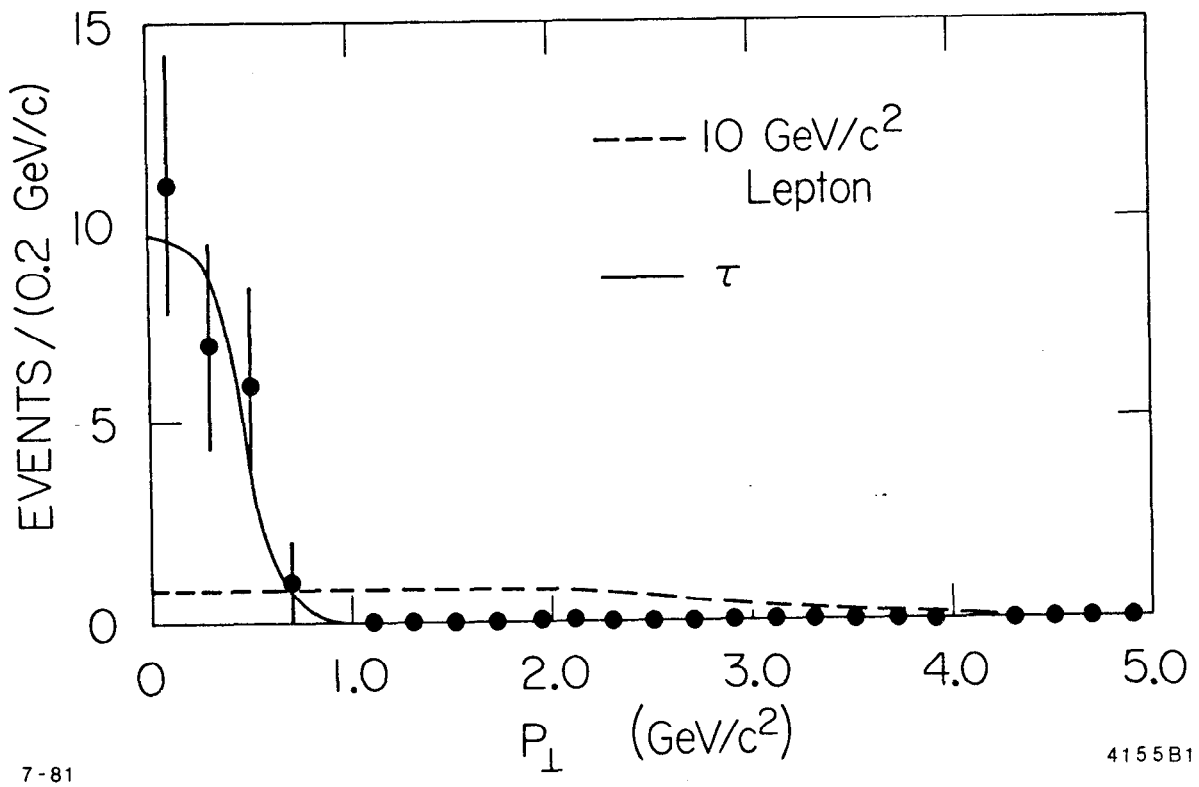

Fig. 19. The transverse momentum for leptons in eμ events is shown. The absolutely normalized prediction of the Monte Carlo for $e^+e^- \to \tau^+\tau^-$ is shown as a solid line and accounts very well for the data. Also shown as a dashed line is the prediction for a heavy lepton of mass 10 GeV/c^2.

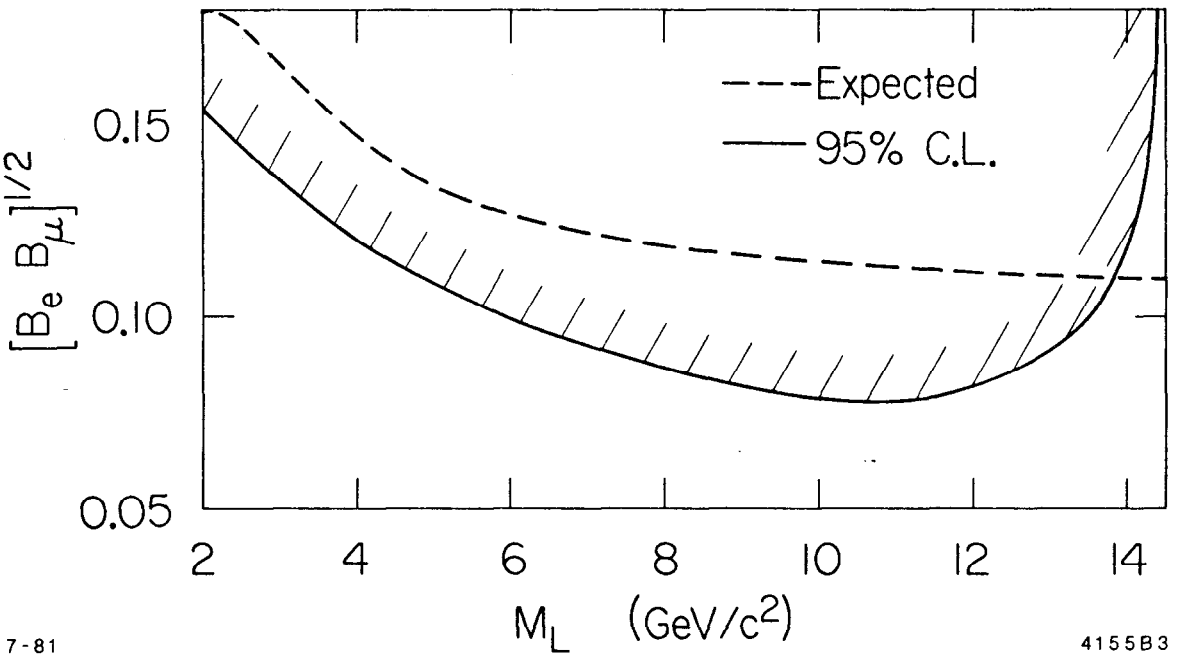

Fig. 20. 95% confidence level limits (solid line) for the product $(B_e B_\mu)^{\frac{1}{2}}$ are shown as a function of the heavy lepton mass. The expectation of a model described in the text is shown as a dashed curve.

For the calculations we have assumed M_c = 1.5 GeV/c^2; all other quarks are massless and Λ = 500 MeV. In this model the τ leptonic branching fraction is 17.9% in good agreement with measurements. (Dropping the α_s/π term, this model is equivalent to saying that above charm threshold the heavy lepton could couple via the W^- to nine distinct weak vertices [$e\nu$, $\mu\nu$, $\tau\nu$, $3\times(ud)$, $3\times(cs)$] and hence B_ℓ = 1/9 = 11%.) Using our model we obtain the results plotted on Fig. 20. Hence we can rule out a new heavy lepton at the 95% confidence limit up to a mass of 13.8 GeV/c^2.

Consider the (unlikely) scenario in which a point, spin 0 boson decayed to $e\nu$ and $\mu\nu$. Such a particle would have the advantage of a two body decay, but the disadvantage of a quarter of a unit of R and a β^3 threshold behavior. Nonetheless we can fit the data of Fig. 19 for this hypothesis and obtain the 95% confidence level upper limits on the mass of such an object as shown in Fig. 21. We have our greatest sensitivity at about 6 GeV/c^2 for which we can place a 95% confidence level upper limit on $(B_e B_\mu)^{1/2}$ of 16%.

TEST OF QED: $e^+e^- \to \gamma\gamma$

A particularly clean test of QED with e^+e^- machines[26] is a study of the reaction

$$e^+e^- \to \gamma\gamma \quad . \tag{6}$$

Tests performed at PETRA/PEP have the advantage of a high-energy, high-momentum transfer probe. In addition the rate for (6) is sufficiently high to make the experiment worthwhile. To order α^3 reaction (6) is described entirely by QED with no effects from electroweak phenomena or vacuum polarization.

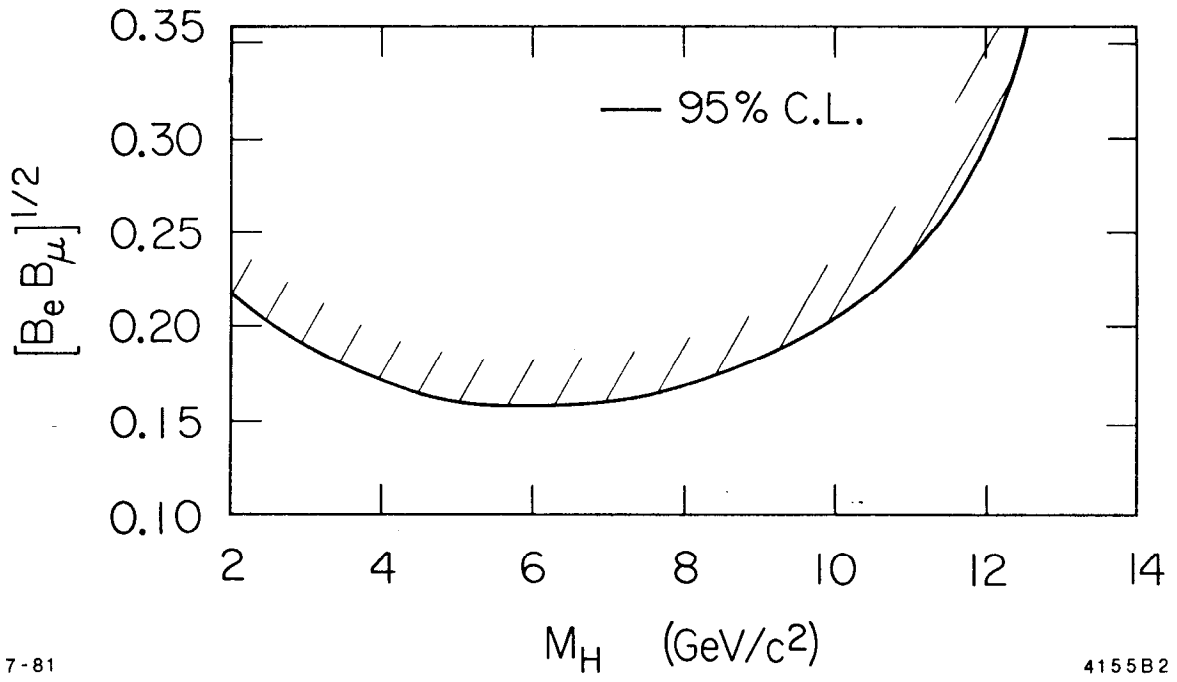

Fig. 21, 95% confidence level limits for $(B_e B_\mu)^{\frac{1}{2}}$ as a function of mass are shown for the hypothesis of the production of a pair of spin 0 bosons each decaying in leptons plus a neutrino.

The data for the analysis comprise 14.4 pb^{-1} and result from the MKII neutral trigger described in the first section of this talk. This trigger has been extensively studied offline using Bhabha events. Since the Bhabha events fire both our neutral and charged trigger, they provide a very handy check on the neutral trigger for $e^+e^- \to \gamma\gamma$. A systematic study of the Bhabhas has led to a measured neutral trigger efficiency of $(98 \pm 2)\%$.

The material surrounding the beam crossing point causes conversions of the photons liberated in reaction (6). Preceding the drift chambers there is 9% of a radiation length of material. There are two possible ways to select events for process (6): (a) select events in which neither photon converts and correct for the ~18% of the events which are lost or (b) select all events with at least one photon which does not convert and sum over all possibilities for the other photon. The systematic errors associated with approach (b) are smaller and, since we wish to make a precise measurement of $e^+e^- \to \gamma\gamma$, we chose this method.

Events are chosen to have at least one well-defined, high-energy photon. Such a photon must be within the fully efficient fiducial volume of the liquid argon calorimeters and have an energy at least as large as $E_{c.m.}/4$. To avoid obvious electron bremsstrahlung, photons close to charged particles are eliminated. The total energy in the liquid argon system is required to be > 19 GeV. The only background to reaction (6) arises from radiative Bhabha events--in particular those events in which there is an internal conversion of one of the photons in the process (6). These events are eliminated easily by requiring that the invariant mass of the two charged particles be > 500 MeV. The net feed-down of this radiative process is computed to be $(1.6 \pm 0.2)\%$ and the

data are corrected for this contamination. A handscan of computer reconstructed event pictures has ensured us that the above cuts are both background free and preserve the desired signal with no discernable losses.

The effects of detector resolution, solid angle losses and uninstrumented "cracks" in the liquid argon calorimeters have been investigated using a Monte Carlo simulation program. As described earlier, raw data are generated and run through the identical analysis passes as the real data. The Monte Carlo model is that of Berends and Kleiss[27] and embodies order α^3 radiative corrections. Kinematic quantities, such as the collinearity of the two photons, have been used as monitors of the simulation performance. In all cases the agreement between the real data and the Monte Carlo data are acceptable.

To present the differential cross section for $e^+e^- \to \gamma\gamma$ the data have been corrected, bin-by-bin, by the ratio of the number of Monte Carlo events to the lowest order calculated cross section:

$$s \frac{d\sigma^0}{d\Omega} = \alpha^2 \frac{1+\cos^2\theta}{1-\cos^2\theta} \qquad (7)$$

where θ is the photon polar angle and $\sqrt{s} = E_{c.m.}$. Since the theory is symmetric in $\cos\theta$, we plot the data in Fig. 22 as a function of $|\cos\theta|$. Each photon in the single or double photon events enters the plot in Fig. 22 with weight 1/2; in events with three photons, each enters with weight 1/3. Also shown on Fig. 22 is the prediction of the Monte Carlo simulation. Agreement between the data and the Monte Carlo events is good.

We may use the $e^+e^- \to \gamma\gamma$ events to search for possible violations of QED. To measure these violations we use the standard form[28] for the QED violation of (7) namely

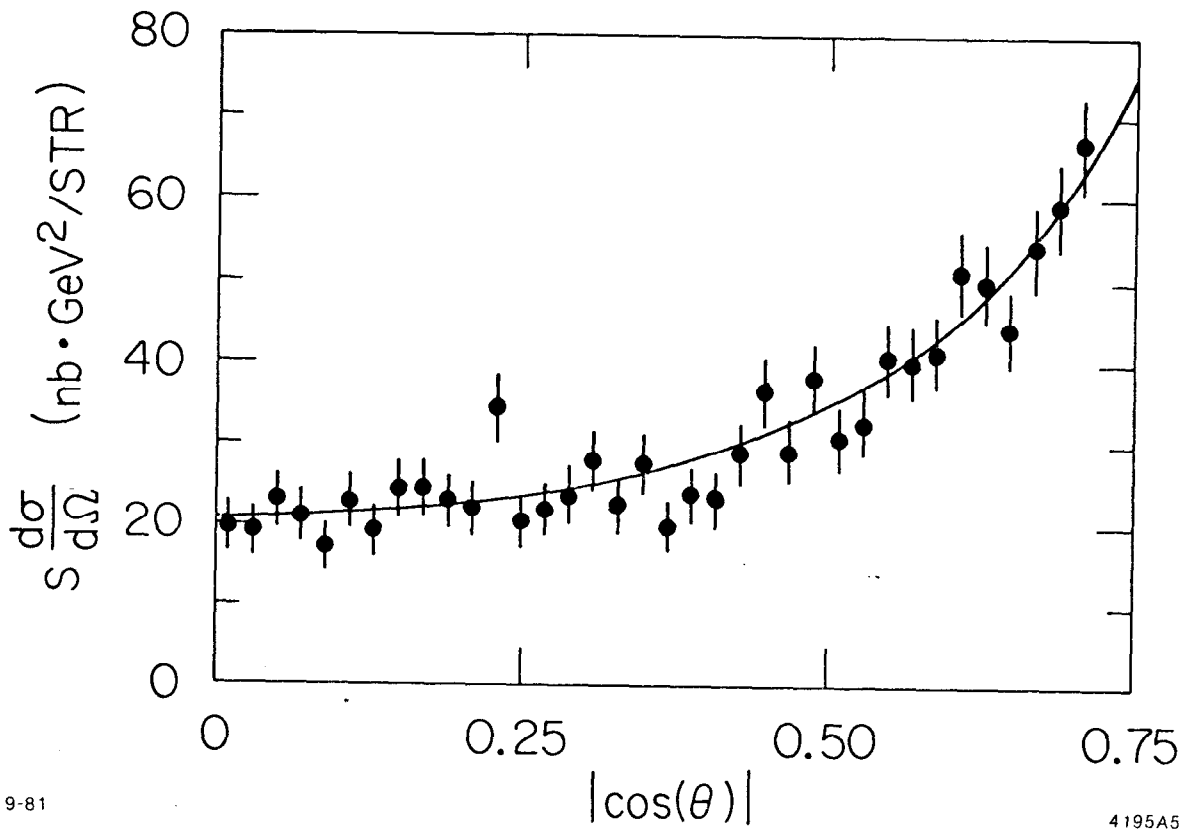

Fig. 22. The cross section s $d\sigma/d\Omega$ for $e^+e^- \to \gamma\gamma$ is shown along with the prediction of QED to order α^3.

$$\frac{d\sigma}{d\Omega} = \left(1 + \frac{s^2}{2\Lambda_{\pm}^4}\left(1 - \cos^2\theta\right)\right)\frac{d\sigma^o}{d\Omega} \quad . \tag{8}$$

The cut-off parameter $\Lambda_+ = M_+/\lambda$ is naturally interpreted as arising from the exchange of a heavy electron of mass M_+ and coupling λ. There is no such natural interpretation for Λ_-. We fit the data to the form (8) and plot the χ^2 as a function of $\Lambda_\pm$. The single parameter in the fit is the luminosity which is allowed to vary within its 2% error. (The luminosity for this analysis is measured using the Bhabhas as seen in the liquid argon barrel calorimeters; see next section). We obtain an excellent fit to the data for no violation ($\Lambda_\pm \to \infty$) namely a $\chi^2 = 25.4$ for 34 degrees of freedom. The 95% confidence lower limits for $\Lambda_\pm$ are deduced from the variation of χ^2 with Λ and are

$$\Lambda_+ = 51 \text{ GeV}$$

$$\Lambda_- = 40 \text{ GeV} \quad .$$

These values are comparable to the limits previously established[29] and listed in Table I. From the results summarized in Table I, it is clear that for $q^2 \sim 1000$ GeV^2, QED is in excellent shape up to order α^3.

TABLE I

Experiment	Λ_+ in GeV	Λ_- in GeV
MARK J	51	49
PLUTO	46	
TASSO	34	42
CELLO	47	44
MARK II	51	40

WEAK-ELECTROMAGNETIC INTERFERENCE

It should be possible, with sufficient integrated luminosity, to see the effects of Z^o exchange at PEP/PETRA energies. Experimentally one uses $e^+e^- \to \mu^+\mu^-$ and $e^+e^- \to e^+e^-$ to observe the modification to the one photon exchange diagrams by the Z^o. One expects to see an asymmetry in the muon angular distribution in $e^+e^- \to \mu^+\mu^-$ and a combined fit to both the lepton channels yields the weak neutral current coupling constants (g_A and g_V) as they apply to the leptons.

We have performed these measurements and the results follow. Because of our limited luminosity the results, while agreeing with the expectation of the standard Weinberg-Salam model, are not significantly different than the pure QED expectations. The PETRA experiments taken singly have the same problem.[30] Recently the data from all five experiments which have run at PETRA have been combined to yield a 3σ effect in the muon asymmetry.[30] This result agrees well with the expectation of the Weinberg-Salam model.

Bhabha and mu-pair candidate events are selected with charged multiplicities from two to six. We retain events with more than two tracks so that we are not sensitive to calculations for the effects of showering in the 9% of a radiation length of material which precedes the drift chamber. Most events have only two charged particles; if an outgoing lepton radiates and the radiated photon converts in the material, four charged tracks result. Six charged particles result from double bremsstrahlung plus conversion and are very rare. The two highest energy tracks are required to have momenta greater than 5 GeV/c and to be collinear to within 200 mr. The latter two cuts eliminate all background from

hadronic events and events arising from the two photon process. The tracks are required to be well contained in the fully efficient regions of the liquid argon shower counters. Each track is classified a muon (electron) if it deposits less (more) than 2 GeV in the liquid argon shower counters. Since a muon deposits on average 280 MeV of energy in a liquid argon module, this is a very efficient and clean classification scheme. Cosmic rays must be eliminated from the mu-pair data and this is done with a time-of-flight cut. The Bhabhas, which can be identified independent of this cut, have been used to measure the $(2.3 \pm 0.2)\%$ loss of mu-pair events resulting from the cosmic rejection. There are 8809 Bhabhas and 652 mu-pair events passing the above selection criteria.

The data for the Bhabha and mu-pair differential cross section are corrected using the Monte Carlo model of Berends and Kleiss[27] (see discussion of $e^+e^- \to \gamma\gamma$ in previous section). As an example, Fig. 23(a) shows the differential cross section for $e^+e^- \to \mu^+\mu^-$. The solid line is QED to order α^3. Although not readily apparent because of statistics, the data have a measurable asymmetry in $\cos\theta$. Fig. 23(b) shows the same data where the QED differential cross section has been subtracted from the data. We have simultaneously fit the differential cross sections for the processes $e^+e^- \to e^+e^-$ and $e^+e^- \to \mu^+\mu^-$ to the QED cross section (to order α^3) plus the weak-electromagnetic interference terms. These cross sections depend only on g_A^2 and g_V^2, and we fit for them. The value of g_A is most sensitive to the muon forward-backward asymmetry and sensitivity to g_V comes from the ratio of the number of Bhabhas to mu-pairs. It should be noticed that this method of obtaining the coupling constants does not require knowledge of the small angle luminosity.

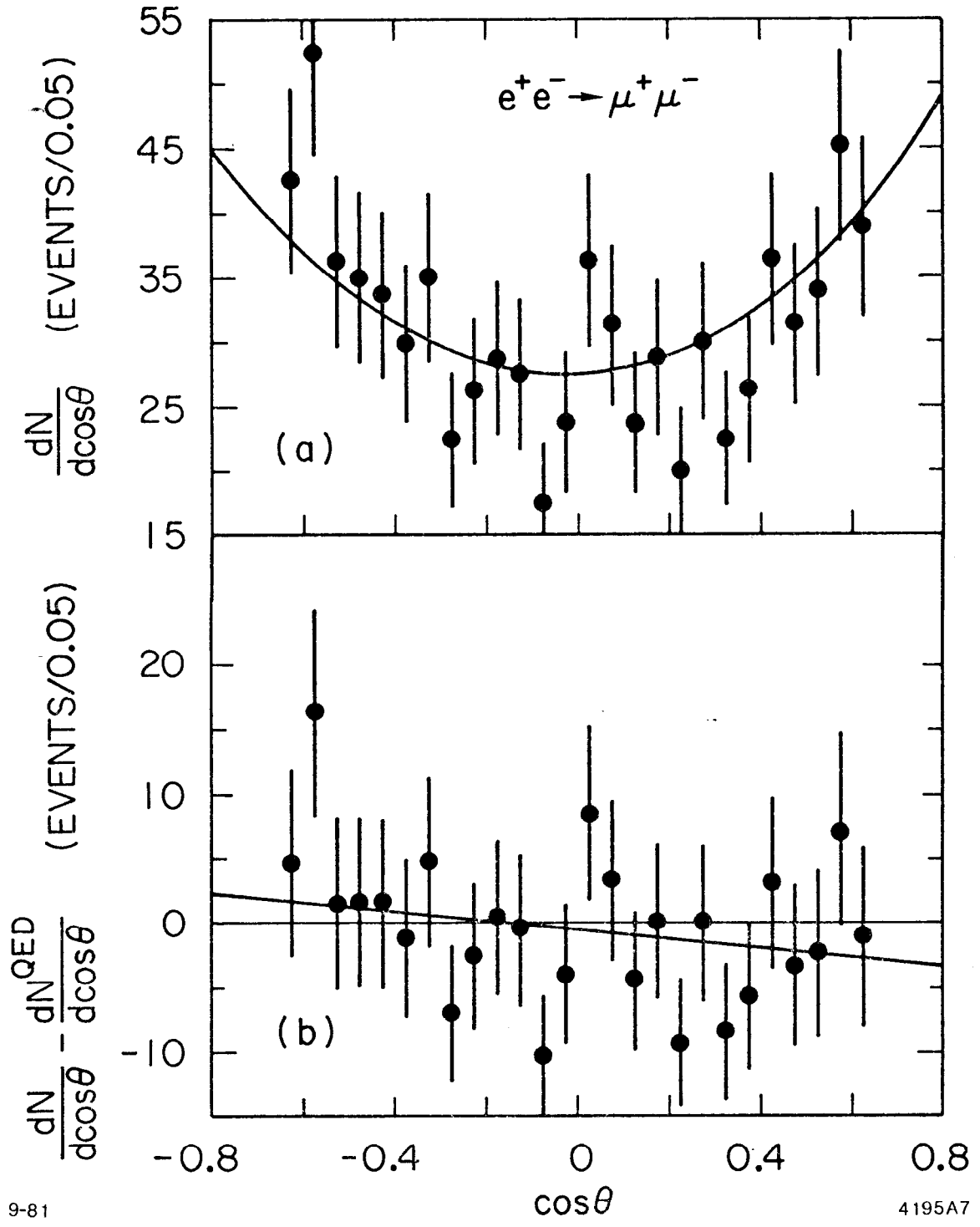

Fig. 23. The angular distribution for $e^+e^- \to \mu^+\mu^-$ is shown in (a) along with the prediction of QED to order α^3. The excess of μ pair events beyond the prediction of QED is shown in (b). The result of a fit to both the μ pair and Bhabha data is shown as a solid line in (b). Although not very significant, an asymmetry is present in the data indicative of electroweak interference.

The results of the maximum likelihood fit are

$$g_A^2 = 0.22 \pm 0.18 \pm 0.03$$

$$g_V^2 = 0.05 \pm 0.10 \pm 0.03$$

where the first error is statistical and the second is systematic. The line in Fig. 23(b) corresponds to the result of the above fit. Fig. 24 is a plot of the 90% confidence contour for G_A^2 versus g_V^2, and compares these limits with the predictions of the standard model and with allowed regions which result from ν-e scattering. Although our data are very consistent with the standard model, they are not inconsistent with pure QED. They do however eliminate, at the 90% confidence level, the one region permitted by the ν-e data. Finally by setting $g_A^2 = 0.25$, as expected in the Weinberg-Salam model, we find

$$0.06 < \sin^2\theta_W < 0.42 \qquad (68\% \text{ C.L.})$$

where θ_W is the familiar Weinberg angle.

All the PETRA experiments have presented the measurements given above. All the data, including the MKII, are consistent but all suffer from large errors. For the reader interested in direct comparisons of the MKII data and the PETRA data, see Ref. 30.

CONCLUSIONS

Data from the MKII at PEP have been presented for the center-of-mass energy $\sqrt{s}$ = 29 GeV. The general features of the one photon annihilation events have been presented. The data are consistent with that of PETRA; by comparison of MKII data at SPEAR and PEP we observe sizeable scaling violations. We have studied energy-energy correlations and have

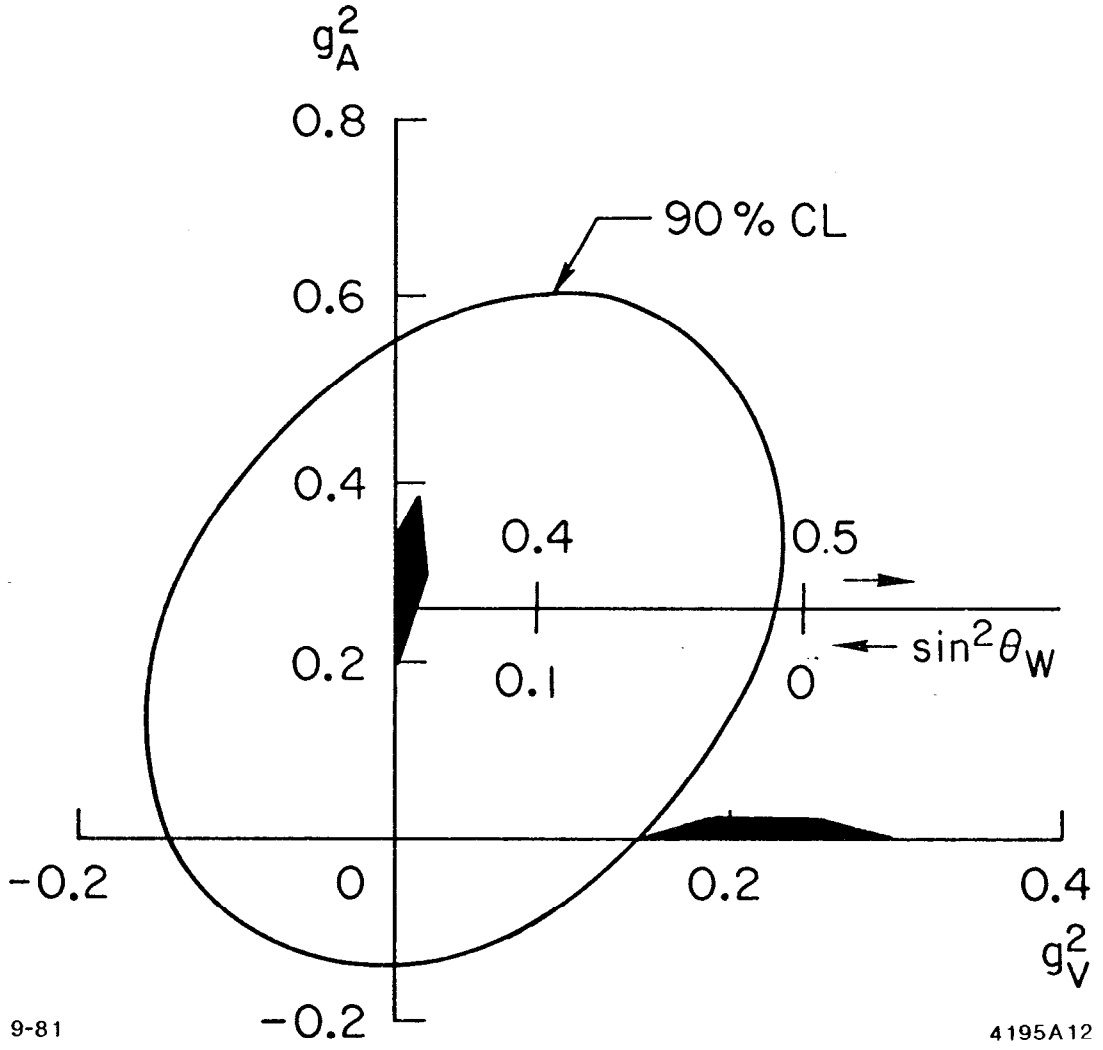

Fig. 24. The 90% confidence level limit contour in the g_A^2, g_V^2 plane is shown. This contour results from a fit to the μ pair and Bhabha data for the quantities g_A^2 and g_V^2. Also shown as shaded areas are the allowed regions obtained from e-ν scattering experiments.

demonstrated that the hadronic jet events are decidedly asymmetric which can be interpreted as evidence for gluon bremsstrahlung. The same asymmetry yields a measurement of α_s. The multijet events, in particular the three-jet events, have been studied using a cluster algorithm. We find that the spin 1 assignment of the gluon fits our data far better than the spin 0 alternative. In addition, comparison with SPEAR data indicates that gluons, in the observed energy range, fragment like quarks. From events containing three-body τ decays, we have found a positive signal in a measurement of the τ lifetime. The measured lifetime agrees, within errors, with the expectations of μ-τ universality. Using e-μ events we have set a limit on the mass of a new heavy lepton. Stringent tests of QED scale breaking have been made using the reaction $e^+e^- \to \gamma\gamma$. Although not statistically very significant, Z^o effects are seen in the reactions $e^+e^- \to \mu^+\mu^-$ and $e^+e^- \to e^+e^-$. These effects permit the measurement of the weak coupling constants g_A and g_V.

REFERENCES

1. D. Cords, Proceedings of XX International Conference on High Energy Physics, Madison, Wisconsin, July 1980.

2. Members of the MKII collaboration at PEP are: G. S. Abrams, D. Amidei, A. Backer, C. A. Blocker, A. Blondel, A. M. Boyarski, M. Breidenbach, D. L. Burke, W. Chinowsky, M. W. Coles, G. von Dardel, W. E. Dieterle, J. B. Dillon, J. Dorenbosch, J. M. Dorfan, M. W. Eaton, G. J. Feldman, M.E.B. Franklin, G. Gidal, L. Gladney, G. Goldhaber, L. Golding, G. Hanson, R. J. Hollebeek, W. R. Innes, J. A. Jaros, A. D. Johnson, J. A. Kadyk, A. J. Lankford, R. R. Larsen, B. LeClaire, M. Levi, N. Lockyer, B. Lohr, V. Luth, C. Matteuzzi, M. E. Nelson, J. F. Patrick, M. L. Perl, B. Richter, A. Roussarie, D. L. Scharre, H. Schellman, D. Schlatter, R. F. Schwitters, J. L. Siegrist, J. Strait, G. H. Trilling, R. A. Vidal, I. Videau, Y. Wang, J. M. Weiss, M. Werlen, C. Zaiser and G. Zhao.

3. R. H. Schindler et al., Phys. Rev. D 24, 78 (1981) and references therein.

4. See for instance B. H. Wiik, DESY 80-129 (1980) or reference 1.

5. T. Appelquist and H. Georgi, Phys. Rev. D 8, 4000 (1973); A. Zee, Phys. Rev. D 8, 4038 (1973); G. 't Hooft, Nucl. Phys. B 62, 444 (1973); M. Dine and J. Sapirstein, Phys. Rev. Lett. 43, 668 (1979); W. Celmaster and R. J. Gonsalves, UCSD-10P10-206,207 (1979); K. G. Chetyrkin, A. L. Kataev and F. V. Tkachov, Phys. Lett. 85B, 277 (1979); and USSR Academy of Sciences, Institute of Nuclear Research preprint D-0178 (1980).

6. J. D. Bjorken and S. J. Brodsky, Phys. Rev. D 1, 1416 (1970).

7. R. Brandelik et al., Phys. Lett. 89B, 418 (1980).

8. The Monte Carlo model used in the MKII analysis is A. Ali et al., Phys. Lett. 93B, 155 (1980); so called HOYER model: P. Hoyer et al., Nucl. Phys. B161, 349 (1979); so called LUND model: T. Sjostrand LUTP 80-3 (1980).

9. See for instance, P. Soding and G. Wolf, DESY 81-013 (1981) or W. Braunschweig, talk at the 1981 International Symposium on Lepton and Photon Interactions at High Energy, Bonn, Germany, August 24-29, 1981.

10. S. Brandt and H. Dahmen, Particles and Fields (Z. Phys. C) 1, 61 (1979).

11. S. L. Wu and G. Zobernig, Particles and Fields (Z. Phys. C) 4, 87 (1980).

12. See for instance D. P. Barber et al., Phys. Rev. Lett. 43, 830 (1979).

13. K. Lanius, DESY 80-36; J. B. Babcock and R. E. Cutkosky, Nucl. Phys. B176, 113 (1980); D. Brick et al., Phys. Rev. D 24, 590 (1981).

14. J. Dorfan, Particles and Fields (Z. Phys. C) 7, 349 (1981).

15. H. Daum, M. Meyer and J. Burger, Particles and Fields (Z. Phys C) 7, (1981).

16. TASSO Collaboration, Phys. Lett. 97B, 453 (1980).

17. J. Ellis and I. Karliner, Nucl. Phys. B148, 141 (1979).

18. Talk of W. Braunschweig at the 1981 International Symposium on Lepton and Photon Interactions at High Energy, Bonn, Germany, August 24-29, 1981.

19. G. Hanson, Proceedings of XIIIth Rencontre de Moriond, Les Arcs, Savoie, France, March 1978, Vol. II, p. 15.

20. D. Schlatter et al., SLAC-PUB-2846, to be submitted to Phys. Rev. Lett.

21. C. L. Basham et al., Phys. Rev. Lett. 41, 1585 (1978)

22. C. L. Basham et al., Phys. Rev. D 19, 2018 (1979).

23. PLUTO Collaboration, Phys. Lett. 99B, 242 (1981).

24. We use the MK II measurement of B_e; C. A. Blocker et al., SLAC-PUB-2820 (1981). Submitted to Phys. Lett.

25. Talk of J. Burger at 1981 International Symposium on Lepton and Photon Interactions at High Energy, Bonn, Germany, August 24-29, 1981, and individually: MARK J Collaboration, MIT-LNS Report #113 (1980); TASSO Collaboration, Phys. Lett. 99B, 163 (1981); and PLUTO Collaboration, Phys. Lett. 94B, 254 (1980).

26. MARK J Collaboration, Phys. Rev. Lett. 43, 1915 (1979);
JADE Collaboration, Phys. Lett. 92B, 206 (1980);
PLUTO Collaboration, Phys. Lett. 94B, 87 (1980;
TASSO Collaboration, Phys. Lett. 94B, 259 (1980);
CELLO Collaboration, Phys. Lett. 103B, 148 (1981).

27. F. A. Berends and R. Kleiss, Nucl. Phys. 186B, 22 (1981).

28. A. Litke, Ph.D. thesis, Harvard University (1970), unpublished.

29. P. Dittman and V. Hepp, DESY 81/39 (1981).

30. Talk of J. G. Branson at 1981 International Symposium on Lepton and Photon Interactions at High Energy, Bonn, Germany, August 24-29, 1981.